Modeling of the Atrioventricular Node during Atrial Fibrillation to Non-invasively Monitor Drug Effects

Katarina In de Betou, F07
Jessica Palmqvist, F07
Department of Electrical and Information Technology

February 25, 2013

Abstract

Objective: To implement a statistical atrioventricular node model which accounts for important electrophysiological properties, and to use the model to investigate the effect of the atrial fibrillation drugs Carvedilol, Diltiazem, Verapamil and Metoprolol. The model uses a maximum likelihood approach to estimate three parameters, that characterize the probability of an impulse choosing either one of the two nodal pathways, the difference in refractory period between these pathways and the prolongation of the refractory periods. *Methods:* The analysis was based on ambulatory recordings. Every participant in the study performed five 24-hour recordings, one for each of the drugs and one without. The model was evaluated on simulated RR intervals to test the parameter estimation, and on the ambulatory ECG to test the accuracy of the estimated PDF. *Results:* The model was accurate when 200 RR intervals or more were present for calculations. The results showed that the estimated PDFs had 77 % agreement with the RR histograms from the ECG signals. For most of the drugs it was possible to see a trend in how they affected the parameters, even though the change was individual for each patient. The parameters were affected differently by the different drugs. *Conclusion:* This study indicates that the presented model can be used to detect antiarrhythmic drug effect in the atrioventricular node in atrial fibrillation patients.

Index terms - Atrial fibrillation (AF), atrioventricular (AV), atrioventricular node (AVN), Carvedilol, concealed conduction, Diltiazem, dual pathways, Holter recordings, maximum likelihood estimation (MLE), Metoprolol, refractory period, RR intervals, statistical modeling, Verapamil.

Contents

Preface

We would like to start with thanking our supervisor Leif Sörnmo for his enthusiasm, constructive feedback and help during this study, and for providing the task to us. We would also like to thank Frida Sandberg who has provided us with important information, the data and algorithms needed to carry out the study and support during the process. And finally a big thank you to Valentina Corino for an inspiring meeting in Milan about statistical AV nodal modeling.

Chapter 1

Introduction

Atrial fibrillation (AF), is the most common cardiac arrhythmia, affecting 0.5-1 % of the general population. It refers to a rapid and chaotic atrial beating of 400-700 beats/minute that causes the ventricles to beat in an irregular way, often with a rate at 140-220 beats/minute. The quality of life is reduced, it can cause other mortal diseases and give rise to high medical costs. The rapid and irregular rate causes the blood to flow more slowly through the atria, and the risk for a blood clot increases, which can lead to a stroke or other damage in the body. Patients diagnosed with AF is therefore often prescribed with blood-thinning drugs to prevent clots from forming. In addition, there are particularly two treatments of AF: controlling the ventricular rhythm or restoring the sinus rhythm. The pathophysiology of AF is complex and not completely understood. It is therefore desirable to develop techniques to quantify AF disease and to guide the treatment. One of the most common tools to investigate AF, or other cardiac diseases, is the electrocardiogram (ECG) that measures the electrical activity of the heart.

Several groups have done experiments to evaluate the possibility to use signal processing to derive more information about AF. There is a variety of methods to analyze the ECG, mostly by looking at the time between consecutive heart beats, i.e. the RR interval. Some methods mentioned in this study are to analyze RR interval histograms and the Poincaré plot, which are both used in this study to estimate interesting parameters of the atrioventricular node (AVN) and to view changes in the RR interval distribution. Estimation and simulation methods, both invasive and noninvasive, have for example been evaluated by Glass et al. [1] and Cohen et al. [2]. This study is based on the model and non-invasive estimation method by Corino et al.

in 2011 [3], to some extent inspired by Cohen.

The aim of this study is to implement a statistical AVN model which accounts for important electrophysiological properties, and to apply it on ECG signals to analyze the effect of different AF drugs. The model treat the AVN as a lumped structure where concealed conduction, relative refractoriness and dual nodal pathways are included. From regular non-invasive ECG signals the RR intervals are retrieved. These are used as input when estimating the AVN properties, using maximum likelihood estimation (MLE). The ECG signals are taken from the RATAF database where patients have taken a 24-hour Holter ECG for each of the four drugs evaluated (Metoprolol, Verapamil, Carvedilol and Diltiazem) and one recording without. All these drugs control the ventricular rate by increasing the AV nodal block and, hence, decreasing the number of atrial activations entering the ventricles.

The anatomical and physiological background of the heart is described in Sec. 2, together with a deeper explanation of the pathophysiology of AF, with different classification schemes and treatments, in Sec. 2.2. The atrioventricular AVN and theories of its behavior is presented in Sec. 2.3. In this chapter the reader is introduced to the physiological concepts that this project are based on. In Sec. 3 earlier work with different models and techniques are described. Sec. 4 gives the mathematical background, describing the theory of Poisson processes, MLE and simulated annealing, all used in this project.

The report continues with a description of the data in Sec. 5 and an description of the method in Sec. 6, going through the process of the Maximum Likelihood estimation and the analysis. The performance of the model was evaluated with different techniques described in Sec. 7. Thereafter the model is applied to analyze drug effects in Sec. 8

Finally, the results are presented in Sec. 9. Sections 10 and 11 contain encountered problems, remarks, suggestions for future work and conclusion.

Chapter 2

Cardiac Anatomy and Physiology

2.1 Heart physiology

2.1.1 Anatomy

The heart is a muscle the size of a large fist [4]. It is divided into two sides, each consisting of two chambers, the atrium and the ventricle. Its primary purpose is to pump oxygen-rich blood throughout the body. Blood is collected in the right atrium from all the veins in the body except from the lungs. When the atria contract, the blood is forced into the right ventricle, which, when filled, contracts and forces the blood into the lungs where carbon dioxide is replaced with oxygen. The oxygenated blood then returns to the left atrium which contracts and forces the blood into the left ventricle, which in turn contracts and empties into the aorta and further to all the organs in the body. The blood then returns to the right atrium through the venous system, and the cycle is complete.

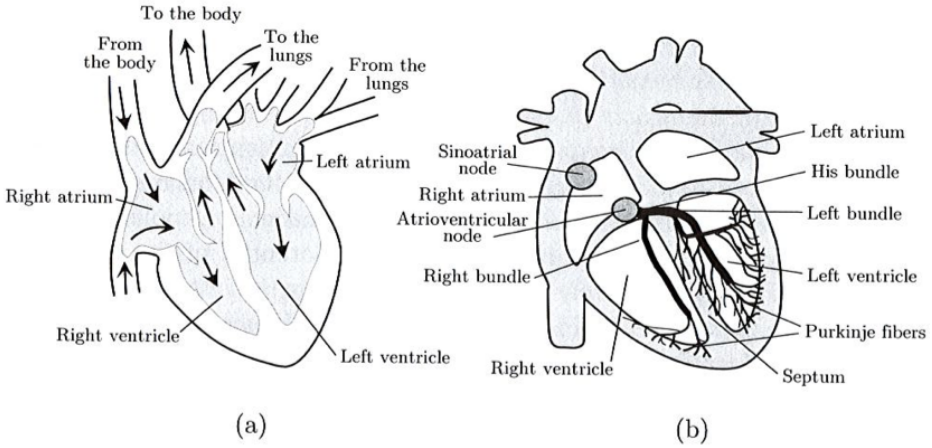

Figure 2.1: Schematic illustration of (a) the heart's anatomy (with arrows showing the direction of the blood flow) and (b) its electrical conduction system.

From an engineering point of view we can consider the heart as a closed, electrically conducting shell of non-negligible thickness that contains electrical sources [5]. The heart is composed by muscle cells with several important properties. They can generate a dramatic change in the electrical potential across the cell membrane, known as an action potential. They can influence neighboring cells to also generate an action potential, producing a moving wavefront. As part of an action potential the intracellular calcium ion concentration increases and the cell contracts. Thus, the electrical and mechanical properties of the heart are closely linked.

Efficient pumping of blood requires that the atria contract first, followed almost immediately by the ventricles [4]. The contraction is trigged by depolarization of the plasma membrane. The excitation of a cardiac cell eventually results in the excitation of all cardiac cells. Each cardiac cycle is composed by two phases, in electrical terms referred to as depolarization and repolarization and in mechanical terms as contraction and relaxation. The impulse propagates through the conduction system of the heart so that the contraction and relaxation of the atria and ventricles can take place with the right timing. The initial depolarization normally occurs in a small group of cells called the sinoatrial (SA) node, which is located in the right atrium. After depolarization and contraction of the atria the impulse is collected

and delayed at the AVN before it enters the ventricles. The delay in the AVN is caused by slower conduction of the impulse in the muscle cells in this region and allows the atrial contraction to further increase the blood volume of the ventricles before they contract. The impulse then enters the wall between the two ventricles at the bundle of His and propagates through rapidly conducting bundles that branches out in the left and right ventricles. Since the electrical behavior of the AVN is of interest in this paper, it will be described in more detail later on.

2.1.2 Electrocardiography

Measuring the electrical activity of the heart is of interest from a diagnostic point of view, since electrical behavior of the heart can alter the contractile behavior and mechanical or chemical changes can alter the electrical pattern [5]. A cardiac action potential generally consists of:

- a rapid activation phase during which the membrane depolarizes
- a longer interval of stable potential, the plateau phase
- a relatively slow repolarization phase during which the potential recovers to its resting value

Once an action potential has been initiated there is a period of time when a new action potential cannot be initiated. This period is called the effective refractory period (ERP) of the tissue. The relative refractory period immediately follows and is the time where initiation of a new action potential is inhibited but not impossible. With electrodes located just outside individual cells the extracellular potential differences between regions of the myocardium can be measured. With the electrode moved further away from the heart, it will sense a larger amount of cardiac tissue and the shape of the signal will change.The ECG recording describes the different electrical phases of a cardiac cycle and represents a summation in time and space of the action potentials generated of millions of cardiac cells. The baseline in the ECG reflects the resting state of the cell and the waveforms corresponds to depolarization and repolarization. Action potentials associated with different regions of the heart are shown in Fig. 2.2. As seen, the depolarization waveforms are steeper and more peaked than the repolarization waveforms. The timing relationship and the related ECG signal is also illustrated [5].

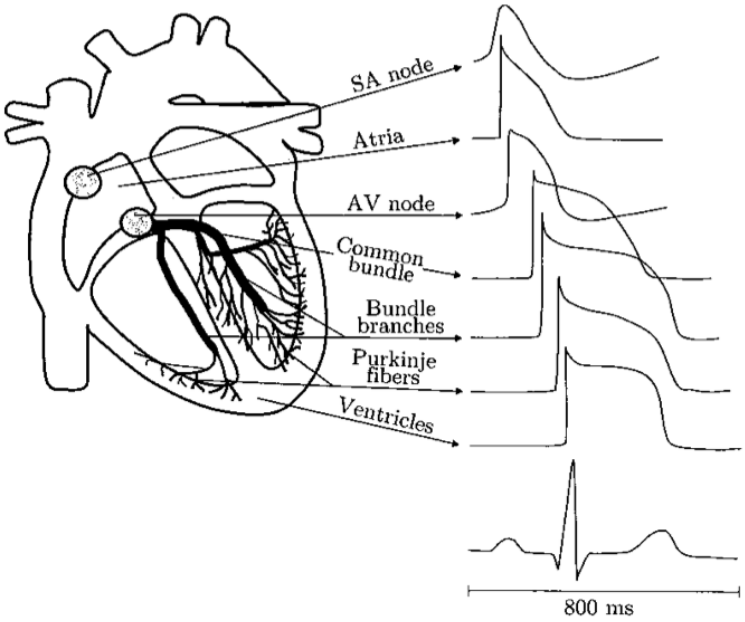

Figure 2.2: Morphology and timing of action potentials from different regions of the heart and the resulting ECG, recorded from the body surface. Reprinted with permission from [4].

A group of cells simultaneously depolarizing can be described as an equivalent current dipole associated with a vector. The vectors describe the time-varying position, orientation and magnitude of the dipole and can be summed to give a dominant vector describing the main direction of the electrical impulse, se Fig. 2.3.

Depending on the location of the electrode the resulting wave can be positive or negative, associated with a vector directed towards or away from the electrode respectively. Generally, the ECG is displayed as in Fig. 2.4. The first wave (P) is associated with atrial depolarization, the second much larger peak (QRS) with the depolarization of the ventricles and the last wave (T) is associated with ventricular repolarization. The R wave is larger than the P wave since the ventricles have a larger muscle mass. The two negative waves (Q and S) corresponds to ventricular depolarization in the walls of the heart, resulting in a vector directed away from the electrode. Up to twelve different leads are used when taking an ECG. Each lead is measured between a pair of electrodes placed at different locations on the chest or body.

Figure 2.3: The vector associated with each group of cells in the myocardium can be summed into a dominant vector describing the main direction of the electrical impulse. Reprinted with permission from [4].

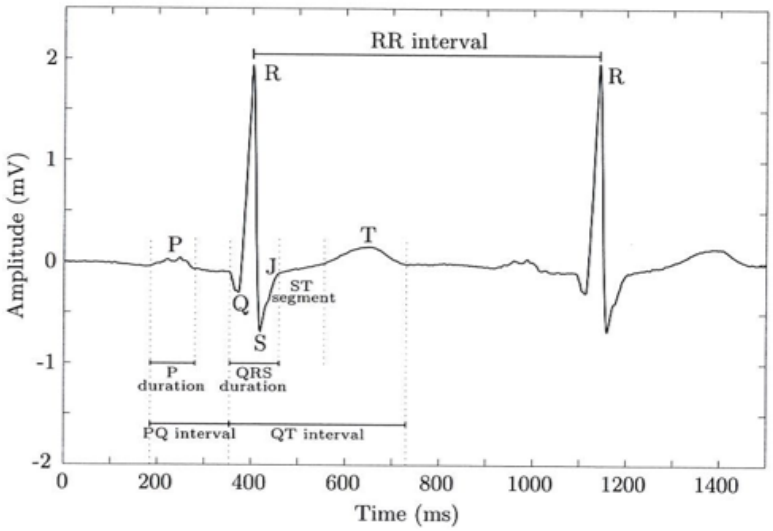

Figure 2.4: Wave definitions of the cardiac cycle and important intervals. Reprinted with permission from [4].

Many cardiac abnormalities cause changes in the electrical behavior, e.g. different arrhythmias. These will alter the shape and size of regional action potentials and cause changes in the body-surface ECG. Arrhythmias arise from many sources and can be very dynamic in nature. The standard ECG plays an important role in clinical medicine. From detecting the heart rate, heart rhythm abnormalities or to find regions of abnormal conduction between the atria and ventricles. But, there are also limitations to the standard ECG. Events in the posterior regions of the heart are not well detected due to the location of the electrodes on the chest. And since the ECG is the spatial integral of many simultaneous events, defects can be canceled out or enhance.

Despite its limitations the ECG is one of the most commonly used diagnostic treatments in clinical practice and thus a preferable tool for deeper analyzes of the electrical behavior of the heart.

2.2 Atrial fibrillation

Atrial flutter and AF are two types of atrial tachycardia produced by increased automaticity in the atrial pacemaker cells [4], [6]. The atriums are unsynchronized with the ventricles and beat at a much faster pace, but since most of the impulses are conducted to the ventricles the resulting heart rate is often 140 to 220 beats/minute. Both atrial flutter and AF are caused by continuing reentry of an electrical impulse in the atria or by ectopic firing, impulses initialized in other parts than the SA. It is manifested in the ECG by an undulating baseline which replaces the P waves. Due to the rapid and irregular rate, blood flows more slowly through the atria and the risk for a blood clot to be produced is increased. If pumped out of the heart, the blood clot can lead to a stroke or cause damage in other parts of the body. Atrial flutter is the more organized arrhythmia of the two, with the atria beating regularly at a rate of about 300 beats/minute. AF, on the other hand, is more rapid and chaotic rhythm with 400-700 beats/minute. This makes the ventricles beat irregularly unlike the ventricular beating during atrial flutter.

The pathophysiology of AF is complex and not completely understood. Genetic predisposition, structural changes and fibrosis, progression of heart disease, inflammation, autonomic dysfunction coupled with electrophysiological abnormalities of the atria, and pulmonary vein sleeves, may all act, to various degrees, as contributors to initiation and maintenance of the fib-

rillatory process. With evolving mapping technologies, stable or unstable reentrant circuits with short cycle lengths, close to the pulmonary vein, have been identified as AF drivers, giving rise to impulses bombarding the AVN. Some of these get through to the ventricles producing a very rapid and irregular ventricular rate.

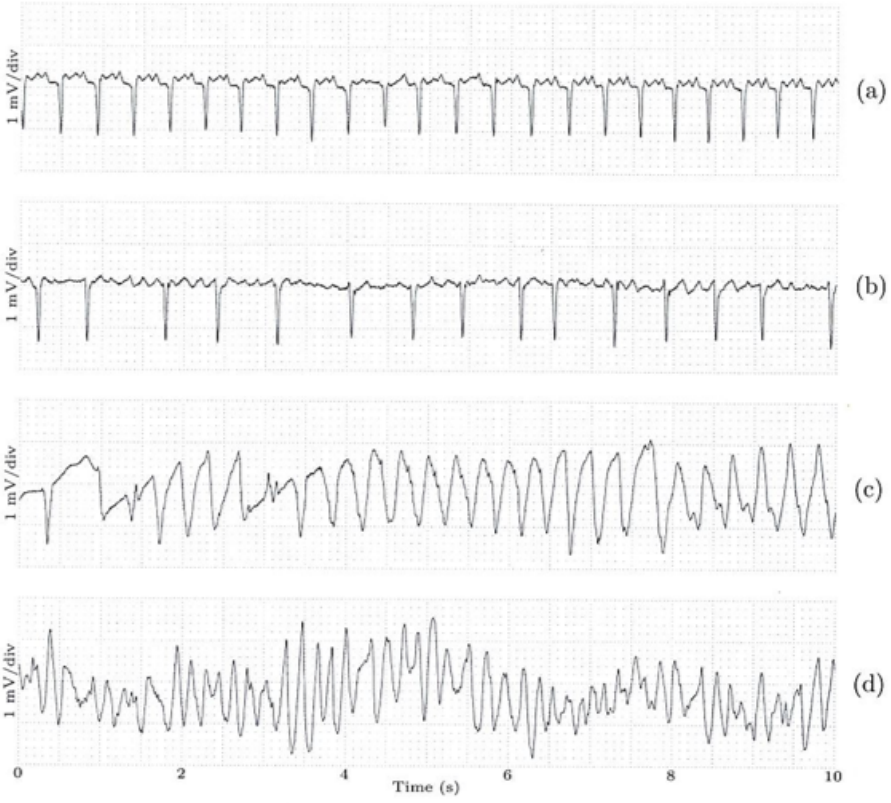

Figure 2.5: Examples of ECG signals for different atrial and ventricular tachycardias. (a) Atrial flutter, (b) atrial fibrillation, (c) ventricular flutter and (d) ventricular fibrillation.

AF is the most common arrhythmia, affecting about 0.5-1% of the general population [7]. Currently, there are two ways to manage AF: to restore and maintain sinus rhythm or to allow AF to continue but keep the ventricular rate under control. The patient selection and management is mainly empirical and does not take the various mechanisms and patterns into account. It is therefore desirable to develop tests the quantify AF disease

state and to guide AF management. Electrograms of fibrillatory waves, alterations of P wave morphology and irregular RR intervals are all considered as expressions of the electrophysiological changes associated with AF.

2.2.1 Atrial activation and mapping

The wavelength concept has been used to describe atrial activation [6]. It is defined as the product of conduction velocity and refractory period. Long wavelengths give rise to larger and fewer wavefronts, while short wavelengths result in smaller circuits that may have implications for arrhythmia susceptibility and stability as well as for therapeutic effects of anti arrhythmic drugs, cardioversion or ablation. Studies on animals as well as humans have been done to examine structural, functional and electrophysiological requirements for AF induction and sustenance and are in close agreement with each other. One common finding was progressive shortening of atrial refractoriness in protocols involving chronic rapid pacing or electrically maintained AF. Daoud et al. and Yu et al. both investigated the effective refractory period (ERP) and found a significant shortening with induced AF.

2.2.2 Classification

Today there is no common agreement on the best AF classification [8]. Several schemes has been proposed, but none includes all different aspects of AF. One scheme is proposed by Gallagher and Camm, and divides AF into paroxysmal, persistent and permanent AF. The first category interrupts spontaneous within 7 days, but often in 24-48 h, the second does not interrupt spontaneously but with therapeutical interventions and the latter where no successful interruptions have been made. AF guidelines published in 2006 divides AF into two groups; first detected AF episode, that can paroxysmal, persistent or permanent, and recurrent AF in the presence of two or more relapses. The classification is important not only for a deeper understanding but also to allow a better comparison of published studies.

2.2.3 Treatment

Some of the general treatments include prevention of thromboembolic complications, control of ventricular rate and restoration of sinus rhythm [8]. Due to the inefficient pumping of blood the risk for thrombosis increases. The thromboembolic risk increases significantly when AF duration exceeds 48 h and thus, patient management varies in relation to arrhythmia duration. Some of the most critical decisions to make in all patients with AF is

how to perform, start and interrupt drug treatment for preventing thromboembolic events. Most patients with AF take anticoagulation drugs, and those with permanent AF often have to continue with the treatment for the rest of their lives.

Control of the ventricular rate is a crucial goal of pharmacological management of AF and drugs acting on the AVN is often used, e.g. Digoxin, beta-blockers and calcium antagonist. Antiarrhythmic drugs or electrical DC cardioversion can be used to restore sinus rhythm. Cardioversion is generally applied to patients with AF duration greater than 48 h. In about 60% of patients where sinus rhythm is restored AF recurs in 6-12 months. Prevention of AF recurrences is therefore a major objective in the treatment of AF patients. However, this treatment suffers from limited efficacy and relevant incidence of side effects of antiarrhythmic drugs, but new promising strategies to evaluate AF recurrences are developing.

2.3 The atrioventricular node

The AVN is a small region of the heart that regulates the relation between atrial and ventricular activations [9]. Over the years different ideas of how the AVN works has been described. For example the refractoriness of this region can be modeled in different ways.

2.3.1 Concealed conduction

One of the theories is about concealed conduction, first used by Langendorf [10] in 1948 to describe how an impulse entering the AVN sometimes fails to transmit it to the ventricles. Concealed conduction within the AVN is often described as the reason for the irregular ventricular rate during AF. The term was initially restricted to include partial or incomplete forms of AV nodal block, where an impulse did not generate a distal response but had an impact on the impulses that followed it, and abortive AV conduction of a premature junctional impulse blocked in both directions. The concept of concealed conduction has grown over the years to explain the relatively slow ventricular rate during AF. It states that the ventricular rate is determined by strength, form, number, direction and sequence of the fibrillatory impulses that reach the AVN and by the electrophysiological properties of the AVN. Long RR intervals are described as a consequence of repetitive concealed anterograde AVN conduction, while short RR intervals corresponds to the functional refractory period of he AVN.

2.3.2 Decremental conduction

Another idea is that of decremental conduction, where an impulse fails to transmit due to a progressive decrease of the action potential as it spreads through the tissue. From the original studies of Hoffman, concluding that the AVN is the site of slow but continuous conduction of electrical impulses from the atria to the His bundle, it has been almost universally accepted as the mechanism responsible for the slowing of conduction and block due to repetitive premature excitation of the AVN. According to Watanabe and Watanabe "AV block occurs because of decremental conduction rather than by a refractory barrier, although the resultant concealed conduction would prolong the refractory period of distant nodal fibers and further modify the conduction pattern." Meijler et al. [9] states that the concept of decremental conduction, as described by Hoffman, only can occur in homogeneous and continuous excitable media, which is not the case for the AVN. Their work is thus critical to this concept and concludes that "although electrotonic modulation of pacemaker activity may not explain some of the phenomena associated with the AVN response to AF, the explanation of Watanabe and Watanabe based on the concept of decremental conduction seems at least equally unsatisfactory".

2.3.3 Electrotonic modulation

The work of Meijler et al. [9] mainly concerns the idea of electrotonic modulation in the AVN and how this idea relate to that of decremental conduction. Electrotonic denotes the spread of current in tissues by electrical conduction, without generation of a new action potentials. They state that the difference between these two is that in decremental conduction the amplitude of the active response decreases gradually until it dissipates completely and is unable to excite tissue ahead of it. In electrotonic transmission, on the other hand, the action potential stops at the site of a block.

An impulse that is blocked within the AVN may induce a subthreshold depolarization just distal to the site of the block. This is caused by electrotonic current flow from depolarized to non depolarized cells and can be manifested at appreciable distances ahead of the block. This effect can, and has been, measured with micro electrode recordings of actions potentials in the AVN during premature stimuli. It has been shown that electrotonic depolarization can have profound effect of the electrophysiological properties of the tissue distal to the block. Experiments to demonstrate this phenomenon has been done by different groups. Antzelevitch and Moe [11] used differ-

ent models of isolated cardiac Purkinje fibers and concluded that concealed conduction may be explained in terms of, what they called, electrotonic inhibition of excitability. Davidenko et al. [12] has also demonstrated in their experiment that while repetitive depolarizing pulses of threshold amplitude elicited action potentials in a 1:1 manner, single brief subthreshold pulses led to transient decays in excitability and even complete failure of subsequent excitation.

More recently Liu et al. [13] carried out experiments in single myocytes from the rabbit AVN along with computer simulations to study the mechanism of electrotonic inhibition and the cellular basis of concealed conduction in the AVN. They found that electrotonic inhibition was the result of partial inactivation of the transient calcium current and that the subthreshold response to prevent subsequent excitation of an AVN cell was increased when the interval between the conditioning subthreshold pulse and the succeeding pulse was shortened, or when the amplitude of the subthreshold pulse was increased. Their simulations with an array of AV nodal cells also showed that an impulse that failed to traverse the AVN caused a delay or block of the following impulse due to subthreshold depolarization that continued downstream of the site of block.

2.3.4 Dual pathways

One property of the AV conduction system is the dual pathway AVN electrophysiology. This term refers to a theory of two different wavefronts that propagate in tandem from the atria to the His bundle. One has a shorter effective refractory period and one has a longer, called the slow and fast pathway, respectively. This phenomenon was first described by Moe et al. [14] in 1950's, but the role the two pathways play in the conduction system of the AVN is still debatable. Moe et al. performed experiments in dogs, turtles, sheep and cats to prove the theory of two parallel AV nodal conduction pathways communicating with each other. Their evidence was based on the excessive delay of very early premature responses in traversing the node, suggesting that a slowly conducting pathway recovers earlier than the normal "fast" pathway. The evaluation of their individual impact on the conduction was ambiguous since the pathway responsible of a particular beat could not be identified. Zhang et al. [15] has introduced the His Electrogram Alternans (HEA), a recording technique that allows identification of the dominant pathway and consequently the evaluation of the role of each pathway. Climent et al. [16] uses the HEA technique to create a

mathematical model of dual pathway AV nodal conduction that accurately reproduced interactions between fast and slow pathway during regular and irregular atrial pacing protocols.

The faster pathway is characterized by longer refractory period and faster conduction velocity, and vice versa for the slower pathway [17]. Since the two pathways differs in conduction and refractory properties they might be affected differently by pharmacological intervention.

Chapter 3

Signal processing - different techniques and applications

In the following chapter different techniques used when analyzing ECG signals from patients with AF are presented. These techniques focus on the AVN and those used later in this study are given more space. Earlier work by different groups are also presented, along with selected results.

3.1 Analyzing ECG with signal processing

One way to describe what happens during AF in the AVN is through signal processing of the ECG signals. There is a variety of methods within ventricular response analysis to do this. The aim with the following paragraph is to describe some of the modern methods of today.

3.1.1 RR interval Histograms

Constructing RR interval histograms can be of interest to evaluate AV nodal conduction properties [8]. These histograms can be produced from ECG recordings of patients with paroxysmal or persistent AF. They can be uni-, bi- or multimodal, where the bimodal histogram by some is claimed to evidence dual AV nodal pathways.

One technique for displaying and analyzing RR interval histograms is the heart rate stratified histogram (HRSH) analysis . Since RR intervals span a wide range of heart rates, this technique gives a more detailed observation of the RR distribution at different heart rate levels. This technique can reveal

information, e.g. bimodality, that is not visually obvious in the unstratified histogram. Before constructing an RR interval histogram, noise and beats not classified as normal are excluded together with the intervals directly before and after. Premature ventricular beats and RR intervals longer than 1.5 s are also excluded.

Histograms are then constructed by dividing the analyzed ECG into segments containing a fixed number of beats. The mean heart rate of each segment classifies the segment into a certain heart rate group. The series are divided into overlapping sequences of length L, according to:

$$\begin{aligned} \mathbf{x}^L(n) &= [x(n)x(n+1)\dots x(n+L-1)]^T, \\ \mathbf{x}^L(n+k) &= [x(n+k)x(n+k+1)\dots x(n+k+L-1]^T, \end{aligned} \tag{3.1}$$

where $x(n)$ denotes the RR interval and k the distance in beats between two consecutive sequences, thus if $k < L$ the sequences overlap.

This technique gives one histogram for each heart rate level, for example in range of 10 bpm, 60-70, 70-80 and so on. Smoothing can be done with a low-pass filtering technique to erase local maxima. The histograms can then be analyzed by visual inspection. The highest and second highest peak are defined as dominant and nondominant. At lower heart rates the peak corresponding to longer RR intervals is dominant and as the heart rate increases the dominance shifts to the other peak. The heart rate at which this occurs is called the *peak dominant change*. The RR values at the peaks are called *slow peak value* (PVS) and *fast peak value* (PVF), here referring to fast or slow RR intervals, not to be confused with the fast and slow AV nodal pathway. The distance between the peaks is called the *peak gap* (PG) and the ratio between the slow and the fast peak is called *peak value ratio*.

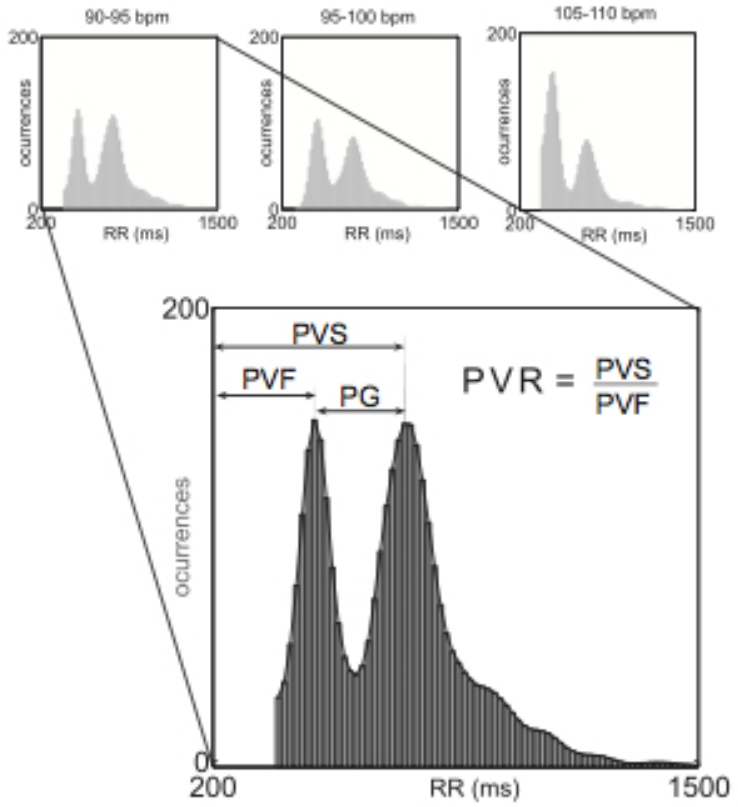

Figure 3.1: Heart rate stratified histogram.

Even though a bimodal histogram is thought to indicate dual AV nodal pathways, it could also be explained by conceal conduction where AV nodal refractoriness differs between proximal and distal region. Also, a unimodal histogram can be associated with dual AV nodal pathways. HRSH have been used by several groups to obtain information about the AVN, some which are mentioned later in this study.

3.1.2 The Poincaré plot

In the Poincaré plot each RR interval is plotted versus the preceding one, which gives information about the sequence of intervals and thus the regularity of the ventricular rhythm [8]. This type of information is not accessible from the RR interval histograms, which makes this technique valuable. As shown in Fig. 3.2 (a), during sinus rhythm each RR interval is strongly

dependent on the preceding one and the intervals are centered around the main diagonal forming an ellipsoid-like pattern. The organized dysfunction of atrial flutter is shown as clusters in the Poincaré plot, Fig. 3.2 (b). The irregularity of RR intervals during AF results in a widely scattered distribution which both indicates the disorganized atrial activity and certain conduction properties of the AVN, Fig. 3.2 (c).

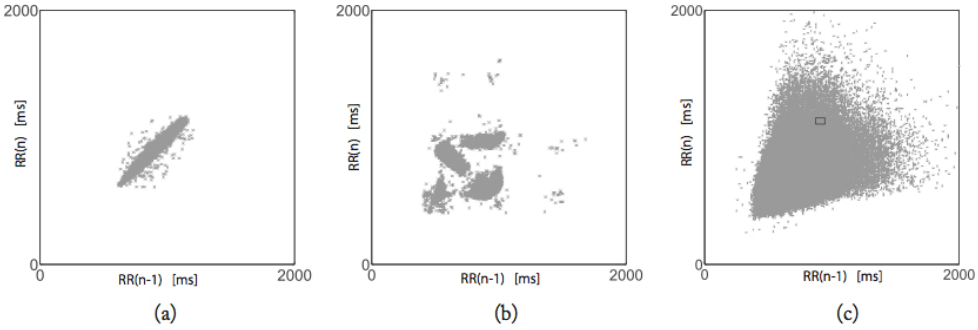

Figure 3.2: Poincaré plot.

The lower envelope is often taken as a measure of cycle length dependence and has been evaluated using different techniques over the years. Manual computation, linear regression and a new method based on the Hough transform has been used by different groups.

The Linear regression line

To find the regression line the horizontal axis is divided into a number of consecutive bins, each with a certain amount of points [8]. The smallest value of each bin is determined and the lower envelope of the plot is found by linear regression fitting to these minimal points. As an example Hayano et al. studied segments of 512 RR intervals each. They divided the axis into 8 bins with 64 points each. For longer segments more points per bin or more bins can be used. The regression line weigh all points equally and is thus not robust against outliers.

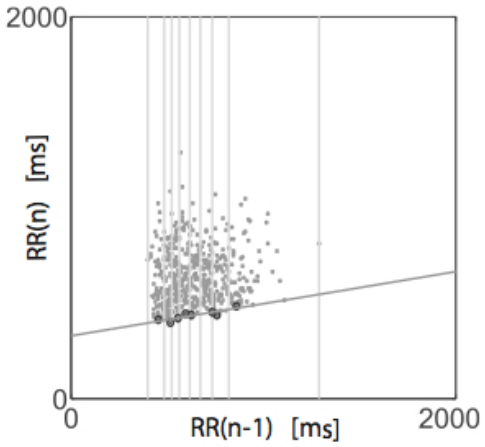

Figure 3.3: Linear regression.

The Hough Transform

With the Hough transform a straight line is detected in an image based on the representation of straight lines in the image space using the line equation $y = mx + c$ [8]. The line is characterized by the parameters (m,c) in the Hough space and since they are unbounded they can also be described with the parameters (ρ , θ), where $\rho = x\ cos\ \theta + y\ sin\ \theta$. To calculate the lower envelope of the Poincaré plot, for each *RR(n-1)* the minimum corresponding *RR(n)* value is detected. Each of these pairs determines the coordinates and is transformed into the Hough space by

$$\rho(\theta) = RR_0 \cos\theta + RR_{min} \sin\theta, \quad -\frac{\pi}{2} \leq \theta \leq \frac{\pi}{2} \tag{3.2}$$

The maximum point in the Hough space, ρ_{max} and θ_{max} is converted to the original space by

$$(x_0, y_0) = (\frac{\rho_{max}}{\cos\theta_{max}}, \frac{\rho_{max}}{\sin\theta_{max}}). \tag{3.3}$$

The lower envelope line is characterized by the slope m and intercept c

$$(m, c) = (-\frac{y_0 - 1}{x_0 - 1}, y_0) \tag{3.4}$$

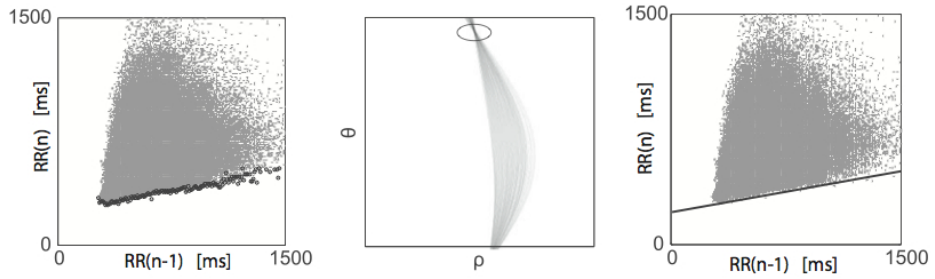

Figure 3.4: Hough transform.

With this method the lower envelope can be evaluated independently of the number of RR intervals, and outliers are automatically excluded.

Once the lower envelope is calculated, the slope and intercept can be used to characterize the FRP and the rate dependence of AV nodal conduction. This technique has shown that the refractoriness and concealed conduction of the AVN may exhibit circadian rhythm, and may therefore be used to obtain more information about the condition of the heart.

3.1.3 Clusters in the Poincaré plot

The Poincaré plot can sometimes exhibit double sector shapes, that has been interpreted as a representation of the dual AV nodal pathways [8]. By fitting two vertices to these sectors, the leftmost one is said to represent the FRP of the slower pathway and vice versa. Another technique with clustering is the histographic Poincaré plot. The number of occurrences for each RR interval pair is represented by gray scale in the plot, where more occurrences result in a darker gray.

There is no evidence that these techniques can be used to determine if dual pathways are present or not, but it may be useful for evaluating drugs effects and AVN modification on the ventricular response.

3.1.4 Time domain analysis

This type of analysis often includes the mean and standard deviation of normal-to-normal (SDNN) intervals, root mean-square differences of successive normal-to-normal intervals (rMSSD), and percentage of interval differences of successive normal-to-normal intervals greater than 50 ms (pNN50) [8]. The technique has been used by different groups to evaluate the effect

of drugs. Both expected drug characteristics and properties not commonly tested has been shown.

3.1.5 Spectral analysis

Due to the irregularity of the ventricular rhythm during AF, which in spectral analysis would result in a huge number of peaks, this technique has not been used commonly [8]. For normal sinus rhythm a noise-like downsloping linear pattern is shown when log-power is plotted against log-frequency. For a patient with AF the spectrum instead divides into two different regions. At lower frequencies the pattern is similar to that of a healthy heart, but for higher frequencies a white noise flat spectrum is shown. This suggests that long-term regulatory mechanisms are still effective in modulating the ventricular response.

3.1.6 Estimating the fibrillation frequency

In the diagnosis and treatment of AF it is of great interest to estimate the frequency of the fibrillation. Due to the spectral overlap between atrial and ventricular activity it is impossible to do a spectral analysis of the ECG signal and cancel out the ventricular activity. To solve this problem more advanced methods have been developed that removes the ventricular activity from the ECG signal. From the residual, rECG, it is then possible to estimate the frequency of the fibrillation.

Residual ECG

One of the most common methods for removing the ventricular activity is Average Beat Subtraction (ABS), originally developed by Slocum et al [18]. In this method an average beat is constructed from the ECG by segmenting the signal into beats, aligning the morphology of the beats in time and taking the average value at each sample. This will cancel out the atrial activity from the average beat, the larger number of beats the better the cancellation. The average beat will then correspond to the ventricular activity and by subtracting it from each beat in the original signal the resulting residual signal will contain the AF. Before subtracting, it is important to align the average beat with the QRST complex in time. The alignment problem can be described by

$$\epsilon^2_{min} = \min_{\tau} \|\mathbf{x} - \mathbf{J}_\tau \overline{\mathbf{x}}\|^2 \tag{3.5}$$

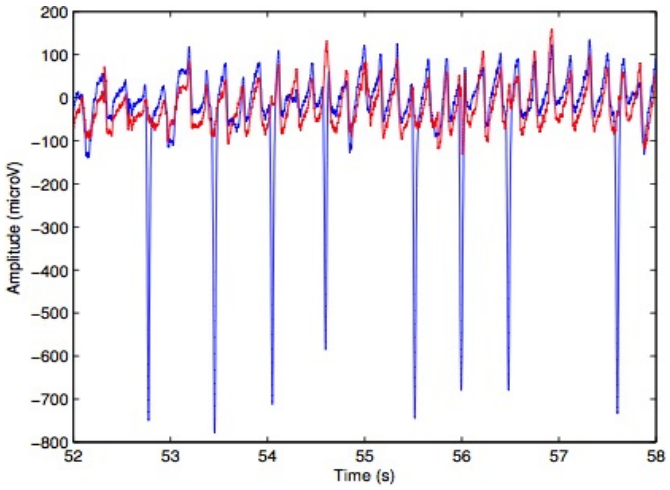

Figure 3.5: This plot shows an EKG where the residual after average beat subtraction is superimposed.

where the vector $\mathbf{x}$ contains the N samples

$$\mathbf{x} = \begin{bmatrix} x(0) \\ x(1) \\ \vdots \\ x(N-1)) \end{bmatrix} \tag{3.6}$$

$\overline{\mathbf{x}}$ is the average beat and $\mathbf{J}_\tau$ is the shift matrix

$$\mathbf{J}_\tau = \begin{bmatrix} \mathbf{0}_{N\times(\Delta+\tau))} & \mathbf{I}_{N\times N} & \mathbf{0}_{N\times(\Delta-\tau))} \end{bmatrix} \tag{3.7}$$

The two matrices $\mathbf{0}$ and $\mathbf{I}$ are the zero matrix and the identity matrix respectively. The minimization problem is thus solved by a grid search over τ finding the N samples of $\overline{\mathbf{x}}$ that gives the best fit to $\mathbf{x}$. After subtraction the resulting residual signal contains the atrial activity. In Fig. 3.5 an example of the residual ECG is shown.

Variations in the orientation of the heart's electrical axis, caused most commonly by respiration, can generate changes in the QRST morphology and the average beat will not fit accurately [19]. This can sometimes cause large QRST residuals. The problem has led to the development of spatiotemporal QRST cancellation. This method uses the multi-lead ECG and introduces shifting and scaling of information between leads to compensate

for these variations. Other variations in the signal has led to further development of ABS. One method uses separate QRS complex and T wave cancellation to compensate for the fact that the QRS complex varies more at different heart rates.The TQ-based fibrillation signal is another method that reduces the influence of AF to get a better estimation of scaling and rotation parameters.

Another common method for QRST cancellation is the Principal Component Analysis (PCA) [19]. This method uses an orthogonal transformation to convert observed, possibly correlated variables to a set of uncorrelated variables called principal components. PCA relies on the assumption that the signal $\mathbf{x}$ is a zero-mean random process, with the correlation matrix, $\mathbf{R_x}$, being equal to the expectation of the squared signal. The principal points are calculated by an orthogonal linear transformation of $\mathbf{x}$. To compute these points the eigenvector equation for $\mathbf{R_x}$ has to be solved. The eigenvector corresponding to the largest eigenvalue relates to the dominant QRST-complex morphology, and the next eigenvectors relates to the dynamics of the QRST complex. A following number of eigenvectors relates to the atrial activity and the remaining eigenvectors relates to the noise in the signal. The ventricular activity can then be subtracted as a linear combination of the eigenvectors corresponding to the QRST complex, or the atrial activity can be extracted with help of eigenvectors corresponding to the atrial activity.

A novel multi-lead method for cancellation of ventricular activity during AF was presented in a recent study by Petrenas et al [20]. The method is based on an echo state neural network which estimates the time-varying nonlinear transfer function between two leads. One lead with atrial activity and one with negligible atrial activity that is used as a reference lead, which is an essential requirement for the method. The network has different sets of weights that define the input, hidden, and output layers of which only the output set is adapted for every new sample to be processed. In this way the network can "learn" how to reproduce specific temporal patterns. In the study this method showed better results than an average beat subtraction method, and is presumed to be very good for QRST cancellation in ECG signals with substantial variation in beat morphology and/or occasional ectopic beats.

Frequency estimation

One way of estimating the fibrillation frequency is by estimating the power spectrum, also known as a periodogram, of the rECG [4]. But the periodogram is a biased estimator with leakage and smearing and does not always give reliable results. A better way is then to estimate the frequency by using Welch's method on the calculated residual. Welch's method divides the signal in the time domain into consecutive segments and then lets these segments overlap, usually 50%. Thereafter the periodogram is calculated for each segment. The final power spectrum from where the frequency can be extracted is created by averaging over these periodograms [21]. By doing this the leakage and smearing effects are markedly reduced. Example of a Welch spectrum can be seen in Fig. 3.6

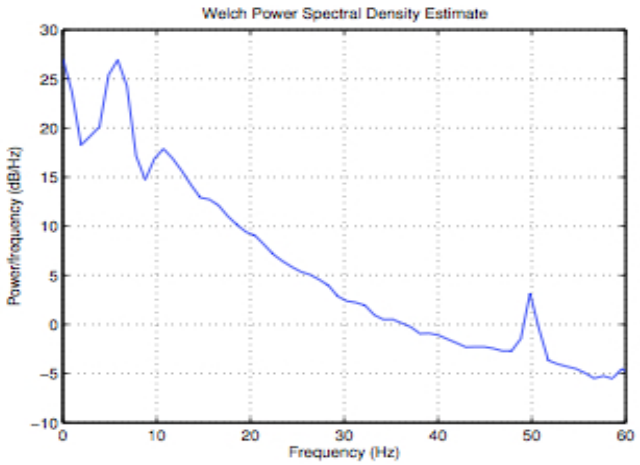

Figure 3.6: A Welch power spectrum. The AF frequency is the first peak, and the second peak is due to network disturbance.

A drawback with using the periodogram is that it precludes the detection of variations in the fibrillation frequency. These changes can be tracked by the short-time Fourier transform (STFT), but the method is known to have rather poor resolution.

Several methods based on different mathematical techniques have been developed to detect variations in the fibrillation frequency while being robust to noise. One a method is based on the hidden Markov model, [22], and it will be explained a bit closer since it will be used in this study. First STFT is performed on the rECG to obtain a sequence of observed frequency states.

Then with an HMM it is possible to detect and exclude frequency estimates that differ significantly from the frequency trend and instead replace them by estimates based on adjacent frequencies. This works because of the Markov models construction of a finite number of states that correspond to a unique set of variables. Each state has predefined state transition probabilities, where the likelihood of a certain state depends only on the previous state. The states are also associated with certain observation probabilities, since the state variables cannot be directly observed. The optimal state sequence is then obtained using the Viterbi algorithm. This algorithm exploits the state transition matrix, incorporating a priori knowledge on AF characteristics, and the observation matrix, incorporating information of the frequency estimation and signal-to-noise ratio. The states of the model correspond to the underlying frequencies, while the observations are determined by the estimated frequency of a specific time interval of the signal. The results from the study showed that the use of HMM improves performance by reducing the root mean square error associated with frequency tracking.

3.2 Mathematical models of the atrioventricular node

Signal processing is an important tool for quantifying AF patterns and properties, but also for investigating the effects of different AF drugs. Several models have been made trying to describe the electrical properties of the AVN and estimate different parameters. Estimation models describe the AVN in a rough way, where only the most important physiological characteristics are accounted for. The point with this is to create a model where the parameters that the model lean upon can be estimated. Another way to use signal processing is by trying to create a model that simulates the AVN behavior as thoroughly as possible. Estimation and simulation models can be based on either non-invasive or invasive measurements of the AVN. The AVN is still not fully understood, and especially the role of its physiology and the rate of AF waves raises questions. The following paragraph mentions some of the more important models along with the properties of the AVN which they take into account.

3.2.1 Non-invasive estimation models

Cohen et al. [2] introduced a model for the genesis of RR interval fluctuations during AF. The main concept of the model is to in a simple way account for

the statistical characteristics of the AVN and produce quantitative results with electrophysiological properties. They assume that the AV junction (AVJ) is bombarded with a series of electrical impulses that arrive randomly in time; hence these atrial impulses are mathematically characterized as a Poisson process. All the temporal and spatial electrical activity in the cells of the AVJ is summed into a hypothetical electrically active cell; the AVJ equivalent cell, AVJEC. This cell has well defined electrical properties and is a device to easier understand the input-output characteristics of the AVJ. It is important to remember that the behavior of the AVJEC does not need to correspond to the electrical activity in any real cell in the AVJ. The action potential is of duration τ, during this time the AVJEC is absolutely refractory. Thereafter the transmembrane potential increases at a constant rate $\dot{V}_4$ from its resting value V_R. For each atrial impulse it increases an extra discrete amount ΔV. When it reaches its threshold value V_T the AVJEC fires initiating a new action potential. The transmembrane potential i visualized in Fig. 3.7.

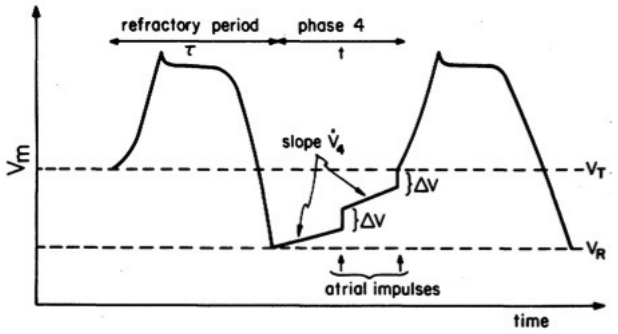

Figure 3.7: The transmembrane potential of the AVJEC according to Cohen et al. [2].

Mathematically the transmembrane potential of the AVJEC can be described by the following expression

$$V_m = V_R + \dot{V}_4 t' + n(t')\Delta V \tag{3.8}$$

Here V_m is the transmembrane potential, t' is the time elapsed since the end of the refractory period, $n(t')$ is the number of the of atrial impulses that have arrived by the time t' and ΔV is the amplitude of the atrial impulses. As mentioned earlier the arrival of atrial impulses at the AVJ is considered

to be a Poisson process and the probability distribution for $n(t')$ is given by

$$p_n = \frac{e^{-\lambda t'}(\lambda t')^n}{n!} \tag{3.9}$$

where λ is the mean rate of arrival for the Poisson process. The criterion for initiation of ventricular activation at time t is $V_m = V_T$. To find the probability distribution for t it is convenient to introduce two new variables

$$\begin{aligned} v &= \dot{V}_4/\Delta V \\ N &= (V_T - V_R)/\Delta V \end{aligned} \tag{3.10}$$

The quantity v is the rate of spontaneous phase 4 depolarization measured in units of ΔV. N is the number of atrial impulses required to depolarize the AVJEC to threshold in the absence of spontaneous phase 4 depolarization ($\dot{V}_4 = 0$). It is now possible to rewrite (3.8) at time t as

$$N = vt + n(t) \tag{3.11}$$

The probability distribution is then deduced by first calculating the probability that the time to reach the threshold is greater than t. This can only occur when $n(t) < N - vt$ and the cumulative probability for that is gotten by summing over n less than $N - vt$. The cumulative probability $P_t(t)$ that the transmembrane potential reaches threshold at or before time t is then one minus that sum. The probability distribution $p_t(t)$ can then be computed by differentiating $P_t(t)$ with respect to t

$$\begin{aligned} p_t(t) = \frac{dP_t(t)}{dt}\frac{e^{\lambda t}\lambda^{n+1}t^n}{n!} + \sum_{k=0}^{N-vt}\frac{e^{-\lambda t}(\lambda)^k}{k!} * \delta\left(t - \frac{N-k}{v}\right) \\ for \quad 0 \leqslant t \leqslant N/v \end{aligned} \tag{3.12}$$

where n is the greatest integer less than $N - vt$. and $\delta(x)$ represents a delta function.

To summarize the simplest form of this model is characterized by four parameters, and the intention was that the model might be utilized to characterize a sequence of RR intervals recorded from a given individual in terms of the numerical magnitude of these parameters:

1. λ - the mean rate at which the atrial impulses bombard the AVJEC.
2. $\Delta V/(V_T - V_R)$ - the relative amplitude of the atrial impulses.

3. $\dot{V}_4/(V_T - V_R)$ - the relative rate of phase 4 depolarization of the AVJEC.

4. τ - refractory period of the AVJEC.

These four parameters are the ones that are altered to compute the best fit between the experimental RR interval histograms and the theoretical ones. Since the refractory period depends on the preceding refractory period, the model is modified to take that into account.

$$\tau_i = \tau_\infty(1 - e^{-T_{i-1}/\tau_\infty}) \tag{3.13}$$

The refractory period of the ith beat, τ_i, is a monotonically increasing function of T_{i-1}, the duration of the preceding RR interval. This modification of the model does not alter the number of adjustable parameter, τ_∞ just replaces τ as the fundamental parameter.

To fit the purpose of the model the AVJ is considered to include not only the AVN but also the automatic tissue of the pre-nodal atrium and the proximal bundle of his. This model accounts for the principal statistical features of the RR interval sequence. The finite time required for impulses to propagate through the AVJ is not explicitly considered in the AVJEC model during AF, with the point that a fixed or random conduction delay will not affect the predicted RR interval since the atrial impulses themselves arrive randomly in time. Although the model is statistical in nature, no well-established statistical parameter estimation procedure was devised. In the paper they used a theoretical best-fit histogram to compare their model with real data. Unfortunately some of the deduced parameters had values that are not physiological possible, i.e. λ was equal to 116 Hz in one histogram. In a subsequent paper the model parameters were determined from the RR series using an ad hoc procedure, however, the results were not very convincing [3].

A more recent model of the AVN during AF was presented by Corino et al. 2011 [3]. This is an extension of Cohens work where further physiological properties are modeled and a statistical ECG-based estimation method for the parameters is presented. In [3], the AVN is treated as a lumped structure that accounts for concealed conduction, relative refractoriness, and dual AV nodal pathways. Atrial impulses are assumed to arrive to the AV node according to a Poisson process. Unless the AVN is refractory each arriving impulse results in ventricular activation (it is suprathreshold), an approach that is different from [2]. No account is made for spontaneous depolarization. The model accounts for dual AV nodal conduction and makes use of an AF rate that is inferred from the ECG. Even though the different properties of the two pathways play a prominent role in ventricular rate control, they are

not routinely evaluated in clinical practice. The model is parsimonious as only six parameters are embraced, which makes the computations relatively smooth. Three of the parameters are estimated independently and three are estimated with a maximum likelihood approach. The output of the maximum likelihood optimization is a set of parameters that provides an electrophysiological characterization of the AVN. All of the parameters are estimated with a general statistical approach. The model in [3], is the base for the study in this paper and therefore it will be described more thoroughly later on in the method, Sec. 6.

3.2.2 An invasive estimation model

With the aim to quantitatively evaluate how a couple of drugs affects six different physiological parameters of the AVN, Glass et al. [1] developed a mathematical model for the AVN during AF. An ad hoc method that included both automatic and manual detection was developed to detect the atrial and ventricular activation times. The mathematical model includes concealed conduction and the conduction times associated with a sequence of conducted beats can be predicted by a simple iterative relationship. Beats that arrive to the AVN while refractory are blocked and lead to an increase in the refractory period that is normally distributed. The model is developed by setting parameters based on comparison between experimental and simulated data. It is difficult to determine the values of all parameters in a six dimensional space. Therefore three of the parameters are fixed at a physiological reasonable value. The model then provides estimates for three quantitative mechanisms of the AVN. The article does not provide information of how the estimates are carried out in further detail.

3.2.3 A non-invasive simulation model

In 2006 Lian et al. [23] described a unified AF - ventricular pacing (VP) model to demonstrate the effects of VP on the ventricular rhythm during AF. The model can be viewed as an extension of [2]; the AVJ is still treated as a lumped structure but more physiological aspects are taken into consideration. A Poisson process simulates the random AF signals. In [23] bidirectional conduction delays is taken into consideration. In addition to the random AF impulses the AVJ can also be affected by retrograde waves induced by VP. When the AVJ fires and generates an activation wave, it also starts an antegrade or retrograde AV delay according to the direction of activation. When both antegrade and retrograde waves are detected in

the ventricle both waves are extinct. The effect that electrotonic modulation by blocked AF impulses has on the RR intervals is also considered in the model. In this article they set their parameters to different values to investigate the effect of the different physiological properties in the AVN. A simultaneous search over all model parameters is not possible, the model consist of sixteen parameters in total. One approach that is suggested is to derive some baseline parameters independently by an ad hoc method, and thereafter with the reduced space dimension try to conduct a search to achieve quantitative data. This was not carried out in the study, and it is not sure whether it will work.

3.2.4 Invasive simulation models

Jørgensen et al. [24] developed a model that incorporates concealed conduction. They also found that a term for concealed conduction is needed to reproduce several statistical features of the ventricular response based on atrial activity. Starting with the input sequence of atrial activations and an initial ventricular activation, an output sequence of ventricular activations is generated iteratively once parameter values are set. The AV conduction time is related to the preceding recovery time through a finite difference equation. An ad hoc method was developed for extracting the activation times of the atrial and ventricular activation complexes. In [2] each atrial input that reaches the AVN during the refractory period contributes to the depolarization of the AVN so that increased atrial stimulation would lead to an increased ventricular response, which is in disagreement with newer studies of the AVN [9]. This is a complement to that study. An atrial activation that arrive at the AVN when it is refractory is blocked and lead to an increment of the refractory period by the amount Δ. The model is built upon five parameters. With an ad hoc approach the model output is compared to recorded ventricular response. The parameters are found by scanning the parameter space, a quite demanding process due to the five-dimensional space. It is not not stated in the article which criterium that is optimized when estimating the parameters. Important to note is that this method was difficult to apply on AF and works better for atrial flutter.

To test the influence of electrotonic modulation in AVN conduction Meijler et al. [9] computed a simplified computer ionic model of the AVN. In this model the AVN is regarded as an area of electrical discontinuities. First they create an oversimplified black-box model of the AV conduction that is composed of a linear array of three excitable elements. Each described by an ionic model of a cardiac cell; the atrium, the AVN and the ventricle.

The conduction is stepwise with the electrotonic currents propagating from cell to cell, with a local action potential at each step. The equations used for the different elements are taken from earlier studies made by Luo and Rudy [25], and Liu et al. [13]. This model was then used to establish the rules of behavior and predictions to be tested in the more elaborated nine-cell model. The more thorough model also consists of a linear array where the cells are separated into the same three. The atrium, AVN and ventricle are now represented by two, five and three cells respectively. The cells were connected with coupling resistances. With proper settings the model simulates a lot of the physiological aspects during concealed conduction and among them electrotonic modulation.

3.3 Previous studies of drugs effect on AF

Several groups have studied the effect of drugs on the AV nodal function. In 1998 Ingemansson et al. [17] published their work where intrinsic AV nodal properties are analyzed during the effect of magnesium ($MgSO_4$) in combination with glucose, insulin and potassium on patients with chronic AF. They used two patient groups, all with chronic AF for at least 3 months. In the first group pharmacological treatment had been unsuccessful and DC conversion had not been attempted and in the second group both pharmacological treatment and DC conversion had been unsuccessful in terminating the arrhythmia. For the first group, both control and intervention recordings were made unlike the second, where only intervention recordings were performed. Both patient groups were submitted to a 24 hour infusion of glucose, $MgSO_4$, Actrapid and K^+ supplement, the second group with a higher dose of $MgSO_4$ and a shorter infusion time. ECG recordings were performed during the investigation, and after a visual inspection determining that only AF with narrow QRS complexes was included, the length of all RR intervals were saved. The intervals were pooled in different groups in a systematic matter and then histograms were constructed for each group of RR intervals. The two highest peaks were classified as dominant and non-dominant, and were associated with the two AV nodal pathways. From the histograms different values, e.g. peak value and peak gap, were extracted and analyzed.

The results showed a significant increase in the peak gap and the RR value for the peak corresponding to the slower pathway, for both patient groups. For the second group, who received a higher dose of $MgSO_4$ PVF (short RR

intervals) also increased, although the increase for PVS (long RR intervals) was more pronounced. Since the only difference in infusion for the two patient groups was the concentration of $MgSO_4$, Ingemansson et al. discussed the possibility that the conduction delay is caused by $MgSO_4$ alone. They also discussed how the drugs may affect the conduction on a cellular level and concluded that the difference for the fast and slow pathway may be due to the possibility that these pathways consists of cells with different ion channel density.

Glass et al. [1] examined the effects of antiarrhythmic drug therapy on AV nodal functions during AF in their work from 2005. The aim was to investigate the effect of Metoprolol and Amiodarone on atrial and ventricular activity in post-surgical patients using three electrodes attached to the muscular part of the right and left atrium. 10 patients were investigated in their study, where three of them did not receive any drug therapy, three received a 24h infusion of Amiodarone, three an injection of Metoprolol and one patient a combination of Metoprolol and Amiodarone. Epicardial signals were acquired and analyzed, and the atrial and ventricular activation times was detected. They also computed histograms over the distribution of the interbeat intervals. In all patients receiving medication the mean ventricular interval markedly increased, while the increase in the mean atrial interval was not as pronounced. This led to the conclusion that the changes in ventricular activation is due to changes in AV nodal properties rather than changes in atrial activation. Their work also indicated that the number of atrial activations that are blocked in the AVN increased following medication, and they note the importance of developing better ways to analyze the effect of blocked beats on the AVN properties.

Chapter 4

Mathematical background

One of the important aspects of this study is a statistical approach to analyzing the ECG signals. Therefore there are some mathematical concepts that are good to be familiar with. The following three sections will explain more about these.

4.1 The Poisson Process

The Poisson process is a point process that evolves without aftereffects. It plays an important role among point processes in continuous time with discrete state space [26]. The Poisson process can be used to model experiments when the events of interests occur at independent random time points but with constant average rate [27]. The events can occur whenever during the given time span, an example of how they can be distributed is shown below in Fig. 4.1.

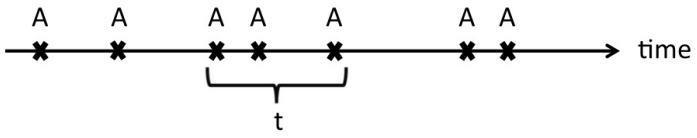

Figure 4.1: Point events that occur randomly in time, where t is an interval of given length.

If we let N be the number of events that take place during a given

time length t, we are interested in the distribution of N [28]. The function $N(t)$ counts all events even if they occur at the same time and is a positive increasing function starting at $N(0) = 0$.

The mean number of events that take place during each time unit of the given time interval is called the intensity, λ, so during a time interval of length t it will occur λt events. If the intensity is constant the process is called homogeneous and if it changes during time, λ(t), the process is called an inhomogenous Poisson process.

The general Poisson process has the following distribution:

$$P(n) = e^{-\mu}\frac{(\mu)^n}{n!} \tag{4.1}$$

where μ is the mean and $N(t) = n$ the parameter for the number of events that has taken place [26]. The mean function of a Poisson process is:

$$\mu(t) = \int_0^t \lambda(\tau)d\tau, \quad t \in \tau \tag{4.2}$$

If the time domain is [0,t] and the process is homogeneous the mean can simply be written $\mu = \lambda t$.

To deduce the distribution for a time interval within the time domain $[0, t]$ we start with the probability law of an inhomogeneous Poisson process [27]. It is completely characterized by the following two principles:

1. For any $t_1 < t_2$ from the time domain τ, the number of point events in the interval $(t_1, t_2]$ has the Poisson distribution with parameter $g(t_2) - g(t_1)$, where g(t), $t \in \tau$, is an increasing continuous function.

2. The number of point events in non-overlapping time intervals are independent random variables.

Since $g(0) = 0$ it coincides with the mean function of the process. With use of the intensity function λ(t) it is possible to write the PDF of a Poisson process in an interval $(t_1, t_2]$, where $N(t_2) - N(t_1) = n$, $n = 0, 1, 2....$, $t_1 < t_2$ as

$$P(n) = e^{-\int_{t_1}^{t_2}\lambda(\tau)d\tau}\frac{[\int_{t_1}^{t_2}\lambda(\tau)d\tau]^n}{n!} \tag{4.3}$$

The PDF for the homogenous process is easy to deduce by eliminating the time dependence for λ. The superposition of several independent Poisson

processes produces the new intensity function of all of the separate intensity functions by simple summation.

4.2 Maximum likelihood estimation

The MLE is defined as the value of θ that maximizes $p(\mathbf{x};\theta)$, the likelihood function, for $\mathbf{x}$ fixed [29]. θ can be either a parameter or a vector, in this text it will denote a parameter but all the assumptions apply for a vector as well. The maximization is performed over the allowable range of θ. Since $p(\mathbf{x};\theta)$ will also be a function of $\mathbf{x}$, the maximization produces a $\hat{\theta}$ that is a function of $\mathbf{x}$. The probability of observing $\mathbf{x}$ in a small volume for a given θ is given by $p(\mathbf{x};\theta)\mathbf{dx}$. In Fig. 4.2 the PDF is evaluated for $\mathbf{x} = \mathbf{x_0}$ and the plotted versus θ. The value of $p(\mathbf{x} = \mathbf{x_0};\theta)\mathbf{dx}$ for each θ shows the probability of finding $\mathbf{x}$ in the region R^N centered around $\mathbf{x_0}$ with volume $d\mathbf{x}$. The possibility of observing $\mathbf{x} = \mathbf{x_0}$ at $\theta = \theta_1$ would be very small and it is more likely that $\theta = \theta_2$ is the true value, since that value yields a higher probability for observing $\mathbf{x} = \mathbf{x_0}$. By using a maximum likelihood approach $\hat{\theta} = \theta_2$ will be the estimate.

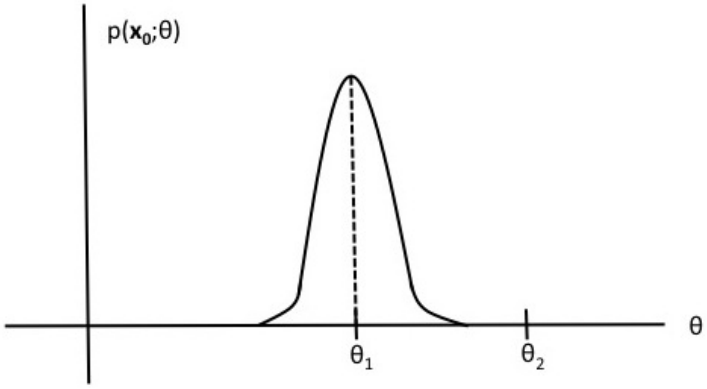

Figure 4.2: The rationale for the MLE.

In general if the PDF for $p(\mathbf{x};\theta)$ satisfies some regularity conditions, then the MLE has the asymptotic properties of being unbiased, achieving the Cramér-Rao lower bound (CRLB) on the variance of the parameters and can be accounted for as fully efficient, and having a Gaussian PDF. It can be said to be asymptotically optimal. In summary the MLE of the unknown parameter θ is for large data records distributed as

$$\hat{\theta} \overset{a}{\sim} N(\theta, I^{-1}(\theta)) \tag{4.4}$$

where $\overset{a}{\sim}$ stands for "asymptotically distributed according to", and $I(\theta)$ is the Fischer information evaluated at the true value of the unknown parameter(s). The regularity conditions require the existence of the derivatives of the log-likelihood function, as well as the Fischer information being nonzero. An analytical expression for the PDF of the MLE is usually impossible, therefore computer simulations are required as a means to assess performance. In practice it is seldom known in advance how large N must be in order for (4.4) to hold and therefore this is an important aspect. Fortunately for many cases the data record lengths are not excessive.

When a closed form expression can not be found for the MLE, a numerical approach employs either a grid search or an iterative maximization of the likelihood function. A grid search is very efficient if the interval where the values of θ can be found is known, but if it is unknown the iterative method is necessary. Some examples of iterative methods are the Newton-Raphson method, the scoring approach and the expectation-maximization algorithm. In general these methods produce the MLE if the initial guess i close enough to the true maximum. If not, the method may not converge, or it may converge to a local minimum. Since the solution is not known a priori it is not known if the attained value actually is the MLE. Nevertheless these methods can produce good results, but it is an aspect that is important to be aware of.

4.3 Simulated annealing

The method chosen to optimize the likelihood function in this study is simulated annealing [30]. Simulated annealing is a probabilistic search algorithm that models the physical process of heating a material and then in a controlled way lower the temperature to decrease defects so it reaches its optimal state, called annealing.

The method of simulated annealing was presented by Kirkpatrick et al. [31]. They showed how the knowledge of statistical mechanics, i.e. the behavior of systems with many degrees of freedom in thermal equilibrium at finite temperature, could be useful for multivariate or combinatorial optimization. The simulated annealing algorithm consists of first melting the system being optimized at a high effective temperature, then lowering the temperature by slow stages until it freezes and no further changes occur. In their study they obtained good results with computational effort scales as

N and even as a small power of N. A slow increase in effort with increasing N is very attractive when dealing with optimizations in many dimensions.

The algorithm in Matlab, which is used in this project, generates a new random point, with a distance from the current point based on a probability distribution with a scale proportional to the temperature, at each iteration [32]. In this way the extent of the search is slowly reduced with each iteration. All new points that lower the energy in the system are allowed, but also to a certain probability, points that raise the energy. The probability of acceptance is

$$\frac{1}{1 + \exp(\frac{\Delta}{\max(T)})} \tag{4.5}$$

where

Δ = new objective - old objective

t = current temperature

For each iteration the algorithm lowers the temperature, storing the best point found so far. The temperature is updated according to

$$T = T_0 \cdot 0.95^k \tag{4.6}$$

where

T_0 = initial temperature of component i

k = iteration number until the system reanneals

Reannealing is a part of the algorithm when a certain number of new points have been accepted and the search starts again at a higher temperature. The annealing parameter is thereafter calculated according to

$$k_i = \log\left(\frac{T_0}{T_i}\frac{\max_j(s_j)}{s_i}\right) \tag{4.7}$$

k_i = annealing parameter for component i

T_0 = initial temperature of component i

T_i = current temperature of component i

s_i = gradient of objective in direction i times difference of bounds in direction i

The algorithm stops when the change in the objective function is small enough. By accepting that some new points might raise the temperature the algorithms explores a global search in the beginning and avoids being trapped early in a local minima. It is still possible for the algorithm to be trapped later on, and therefore it is important to carry out several computations and compare the results to make sure that the generated result actually is the one that minimizes the system energy. The algorithm can be used to find both unconstrained and bound-constrained minimum to functions with several variables. In this study the bound-constrained version is used.

Chapter 5

Dataset

The ECG signals used in this study are taken from the RATAF database [33]. It stands for RATe control in Atrial Fibrillation and started in april 2006 at the Asker & Baerum Hospital in Norway. 60 patients were included, both male and female, all over 18 years old and all with persistent or permanent AF with a ventricular rate over 80 beats/min at rest and/or over 100 beats/min average at daytime. The aim was to compare the effect of Metoprolol 100 mg once daily (o.d.), Verapamil 240 mg o.d., Diltiazem 360 mg o.d. and Carvedilol 25 mg o.d. on reducing ventricular rate during AF. The patients have received the drugs in a random sequence, from patient to patient, and each one was administered for 3 weeks to ensure that a steady-state drug concentration was attained and to provide a washout of the previous treatment. The primary outcomes measured were ventricular rate, working capacity and quality of life. 24-hour Holter ECG recordings were performed for each of the drugs and one without, used as baseline. All recordings were performed under ambulatory circumstances and three leads taken from the chest were used for further analysis.

The drugs were either beta blockers or calcium channel blockers [34]. All these drugs act to control the heart rate, rather than restoring the heart rhythm, by increasing the level of block in the AVN and thus decreasing the number of impulses conducting through the ventricles. Calcium channel blockers work by blocking voltage-gated calcium channels in the cardiac muscle cells leading to a reduction in muscle contraction. Beta and alpha blockers block specific receptors in the cells. Metoprolol and Carvedilol are both beta blockers, the latter also with alpha blocking activity, Verapamil and Diltiazem are both calcium channel blockers.

Chapter 6

Methods

A maximum likelihood approach is applied to estimate a number of parameters from recorded ECG signals. An important aspect is that all of the data needed for the analyze is possible to achieve non-invasively. The parameters to be estimated are the maximal functional refractory period of the AVN, the difference in functional refractory period between the two pathways and and the probability for the signal to take the shorter pathway.

The scope of the project is to:

- *Implement an MLE.* The first step in the MLE is estimation of the input parameters, a procedure that is already constructed by Corino et al. [3]. The second step is the optimization of the output parameters, which is the focus in this study. It is important that the algorithm does not get stuck in local maxima and that the output parameters are assigned physiologically acceptable values.

- *Analyze recorded ECG signals.* This part include deciding upon which modifications that have to be done to the MLE so that the output is reliable parameters to use for further analysis. The model has to account for both judging input parameters and output parameters as reliable. Within this part it is also of importance to decide which data to be saved for the drug analysis.

The following four sections will describe the foundation and statistical properties of the model more thoroughly, and how the estimations are performed. A detailed description of how the model is applied can be found in chapter 7 and 8.

6.1 The maximum likelihood estimator

The model used in this paper is the model described in the work of Corino et al. from 2011 [3]. As mentioned earlier, in their model the AVN is treated as a lumped structure which accounts for concealed conduction, relative refractoriness and dual pathways. From the ECG the arrival rate of the atrial impulses λ and the minimal time for the deterministic part of refractory period τ_1^{min} are estimated. These parameters are then used together with the RR intervals in the ML estimator to get the wanted output parameters, the probability α, the time difference between the to pathways $\Delta\tau$ and the maximal refractory period τ_p^{max}.

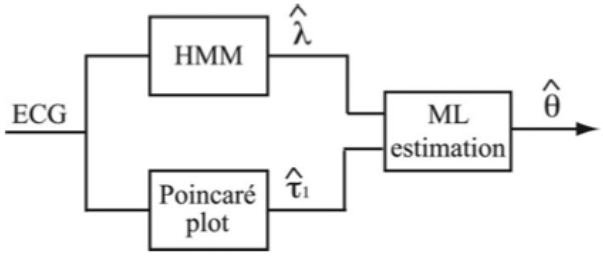

Figure 6.1: Block diagram of the estimation model.

6.1.1 Probability density function

The atrial impulses are assumed to arrive to the AVN according to a Poisson process with mean arrival rate λ. Each impulse is supra threshold and thus results in ventricular activation unless it is blocked by a refractory AVN. The length of the refractory period is defined by a deterministic part τ and a stochastic part τ_p. The deterministic part can assume two values, τ_1 and τ_2 characterizing the to pathways. The stochastic part models the prolongation due to concealed conduction and relative refractoriness and is assumed to be uniformly distributed in the interval $[0,\ \tau + \tau_p^{max}]$. Where τ_p^{max} is the maximal prolongation, identical for both pathways.

Fig. 6.2 illustrates how the refractory period is modeled. In segment A all arriving impulses are blocked, in segment B the probability for an impulse to pass through is linearly increasing and in segment C all impulses pass through to the ventricles since the refractory period is over.

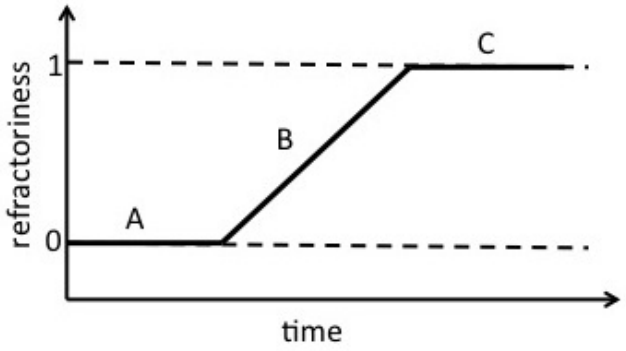

Figure 6.2: Refractoriness

The lower value 0 denotes total refractoriness and this can also be described with the function β_i(t) that characterizes the refractoriness of the i :th pathway as

$$\beta_i(t) = \begin{cases} 0, & 0 < t < \tau_i \\ \dfrac{t - \tau_i}{\tau_p^{max}}, & \tau_i \leq t < \tau_i + \tau_p^{max} \\ 1, & t \geq \tau_p^{max} \end{cases} \tag{6.1}$$

t denotes the time elapsed since the earlier ventricular activation and the pathways $i = 1, 2$.

The probability for an impulse to take the either one of the pathways is defined as

$$p(i) = \begin{cases} \alpha, & i = 1 \\ 1 - \alpha, & i = 2 \end{cases} \tag{6.2}$$

Atrial impulses that are not blocked in the AVN arrive according to a Poisson process with the intensity function $\lambda\beta_i$ (t) that characterizes the time-dependent refractoriness. With the assumption that AV conduction is incorporated into β_i(t), a ventricular activation immediately follows a non blocked atrial impulse. Thus, ventricular activation also occurs according to a an inhomogeneous Poisson process with the same intensity function, $\lambda\beta_i$(t).

The PDF that characterize the non blocked impulses is defined as

$$p_t(t_n) = \frac{\lambda\beta(t)}{(n-1)!}\left(\int_0^t \lambda\beta\tau\right)^{n-1} \exp\left\{-\int_0^t \lambda\beta(\tau)d\tau\right\} \tag{6.3}$$

for the arrival time of the n:th impulse, here denoted t_n. Due to the fact that ventricular activation occurs immediately after the first non blocked atrial impulse, the PDF of the time between two consecutive ventricular activations x is given by

$$p_x(x) = p_t(t_1) = \lambda\beta(x)\exp\left\{-\int_0^x \lambda\beta(\tau)d\tau\right\} \tag{6.4}$$

Since β_i(t) can denote β_1(t) or β_2(t) depending on the pathway, the PDF is composed by two parts

$$p_x(x) = \alpha p_{x,1}(x) + (1-\alpha)p_{x,2}(x) \tag{6.5}$$

where

$$p_{x,i}(x) = \lambda\beta_i(x)\exp\left\{-\int_0^x \lambda\beta_i(\tau)d\tau\right\} \tag{6.6}$$

When inserting (1) in (6)

$$p_{x,i}(x) = \begin{cases} 0, & x < \tau_i \\ \dfrac{\lambda(x-\tau_i)}{\tau_p}\exp\left\{\dfrac{-\lambda(x-\tau_i)^2}{2\tau_p}\right\}, & \tau_i \le x < \tau_i + \tau_p^{max} \\ \lambda\exp\left\{\dfrac{-\lambda\tau_p^{max}}{2} - \lambda(x-\tau_i-\tau_p)\right\}, & x \ge \tau_i + \tau_p^{max} \end{cases} \tag{6.7}$$

Since the ventricular activations are assumed to occur according to a Poisson process, the time interval between two consecutive activations are independent and the joint probability of a RR series is given by

$$\begin{aligned} p_x(x_1, x_2, ..., x_M) &= \prod_{m=1}^{M} p_x(x_m) \\ &= \prod_{m=1}^{M} (\alpha p_{x,1}(x_m) + (1-\alpha)p_{x,2}(x_m)) \end{aligned} \tag{6.8}$$

where $p_{x,1}(x_m)$ and $p_{x,2}(x_m)$ is given by (7).

6.1.2 Input parameters

To be able to use the PDF for the optimization there are some parameters that first need to be estimated. The statistical approach with the Poisson process demands that the RR series are de-correlated, since the RR intervals are not completely independent from each other. Taking this into consideration a functional dependence of τ_i on the previous RR interval is also incorporated in the model. It is enough to estimate the shortest possible AV nodal refractory period, τ_1^{min}. The last parameter that is estimated independently is λ. All this is only done for the real ECG signals. The simulated RR series have independent RR intervals and λ has a fixed mean value.

Estimation of τ_1^{min} and de-correlation of the RR series

Since the preceding RR interval is needed for estimation of the AV nodal refractory period τ_1 this parameter is estimated independently of the other model parameters. The deterministic part of the refractory period depends on the preceding RR interval, so that a longer RR interval is followed by a longer refractory period and vice versa. In this study the lower envelope of the Poincaré plot characterizes the functional dependence. In Fig. 6.3 the current observed RR interval x'_m is displayed versus the preceding interval x'_{m-1}, where x'_m is defined as the time between the $(m-1)$th and mth ventricular activation.

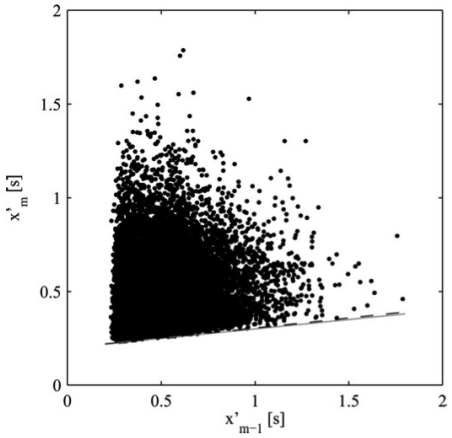

Figure 6.3: Poincaré plot of simulated RR intervals with $\lambda = 7$ Hz, $s_\tau = 0.1$, $\tau_1^{min} = 0.1$ s, $\alpha = 0.7$, $\Delta\tau = 0.2$ s and $\tau_p^{max} = 0.1$ s. The solid line is the lower envelope of the plot.

To estimate the lower envelope the Hough transform to detect straight lines in images is used. First the Poincaré plot is discretized with a bin size of 20 ms, see Fig. 6.4. After this the edges are extracted using the Sobel approximation of derivatives which return edges at those points where the gradient is maximum, see Fig. 6.4

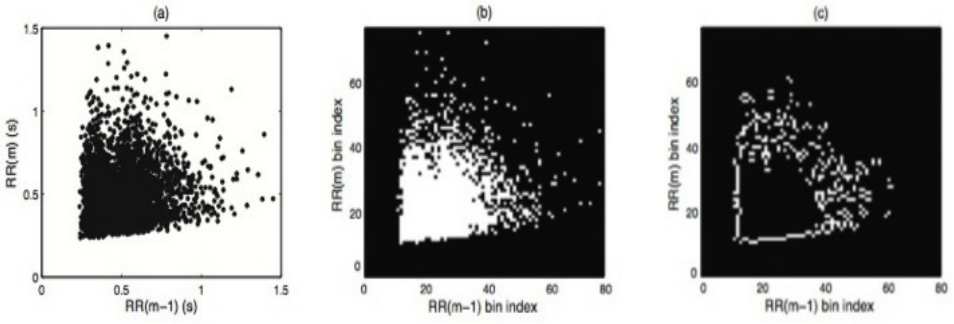

Figure 6.4: Description of the different stages in the Hough transform from a recent article by Corino et al. [35].

In finding the lower envelope of the Poincaré plot the slope is constrained to be within the interval [0, 0.5] and the intercept to be positive. The line

that satisfy this criteria and is closet to the minimum points of the edge points of the image, in a the mean square error sense, is taken as an estimate of the minimal refractory period τ_1^{min} and the slope of the line is denoted s_τ. With these parameters an estimate of the refractory period $\tau_{1,m}$ of the mth activation is possible from the linear relationship:

$$\tau_{1,m} = \tau_1^{min} + s_\tau x'_{m-1} \tag{6.9}$$

Estimating the longer refractory period $\tau_{2,m}$ is identical to estimating a fixed duration $\Delta\tau$, if we assume that s_τ is identical for the two refractory periods.

$$\begin{aligned} \tau_{2,m} &= \tau_2^{min} + s_\tau x'_{m-1} \\ &= (\Delta\tau + \tau_1^{min}) + s_\tau x'_{m-1} \\ &= \Delta\tau + \tau_{1,m} \end{aligned} \tag{6.10}$$

The parameter $\Delta\tau$ is one of the parameters that will be estimated later on in this analyze. From the ECG signals it is, as mentioned above, possible to estimate the slope of the lower envelope of the Poincaré plot for the signals, s_τ. The RR series can now be de-correlated by the following linear transform

$$x_m = x'_m - \hat{s}_\tau x'_{m-1} \tag{6.11}$$

The resulting series are the ones used in the optimization. The interdependence of successive RR intervals has been reduced in the modified series x_m and the stochastic model assumption in (6.8) becomes more valid. This also results in that the parameter τ_1 in (6.7) is estimated with τ_1^{min} and τ_2 with $\tau_1^{min} + \Delta\tau$.

Estimation of λ

The arrival rate λ is also determined independently from the estimation of the ventricular parameters. It is derived from the ECG using spatiotemporal QRST cancellation. The AF frequency is thereafter tracked on a short-term basis using a method based on a hidden Markov model (HMM). A first estimate of λ is given by the median value of the AF frequency estimates computed over the analyzed ECG segment length, λ_{AF}. But this approach does not account for the fact that there is a minimum time interval δ between successive impulses arriving to the AVN. This estimation produces an underestimate value of λ and therefore the arrival rate is modified to

$$\lambda = \frac{\lambda_{AF}}{1 - \delta\lambda_{AF}} \tag{6.12}$$

The Poisson-distributed impulses are now not allowed to arrive closer than the interval δ and this is the parameter inserted into the log-likelihood function in (6.15). In this study it is assumed that the atria depolarize again after $\delta = 50$ ms. The expression in (6.12) is easy to derive. For a Poisson process we have that that during the interval $[0, T]$ with the total number of N impulses $\lambda = N/T$. During the same time interval $\lambda_{AF} = M/T$ reflects that fewer impulses ($M < N$) arrive to the AVN. During the interval δ it is expected that $\delta\lambda M$ impulses occur. The difference between N and M is given by

$$\lambda T - \lambda_{AF} T = \delta\lambda M \tag{6.13}$$

The expression given in (6.12) follows from solving λ_{AF} for (6.13). The introduction of δ produces a right-shifted PDF for the arrivals of the atrial impulses to the AVN. If for example $\delta = 50$ ms and $\lambda_{AF} = 6$ Hz we have that $\lambda = 8.6$ Hz, which is the value used later on in (6.15).

6.1.3 Optimization process

The aim with the optimization is, as mentioned above, to estimate the three model parameters

$$\theta = [\alpha \quad \Delta\tau \quad \tau_p^{max}]^T \tag{6.14}$$

where

α = the possibility that the signal takes the shorter pathway, τ_1.

$\Delta\tau$ = the difference in the deterministic part of the refractory period between the shorter, τ_1, and the longer, τ_2.

τ_p^{max} = the maximal stochastic part of the refractory period.

To optimize the joint likelihood function as it is demands a lot of computational effort and therefore we instead optimize the logarithm of the likelihood function

$$\hat{\theta} = \arg \max_{\theta} \log\, p_x(x_1, x_2, ..., x_M|\theta; \hat{\lambda}, \hat{\tau}_1^{min}) \tag{6.15}$$

where

$$
\begin{aligned}
&\log\ p_x(x_1, x_2, ..., x_M|\theta; \hat{\lambda}, \hat{\tau}_1^{min}) \\
&= \log \prod_{m=1}^{M} p_x(x_m|\theta; \hat{\lambda}, \hat{\tau}_1^{min}) \\
&= \sum_{m=1}^{M} \log(\alpha p_{x,1}(x_m|\theta; \hat{\lambda}, \hat{\tau}_1^{min}) + (1-\alpha) p_{x,2}(x_m|\theta; \hat{\lambda}, \hat{\tau}_1^{min}))
\end{aligned}
\tag{6.16}
$$

In [3] no closed-form solutions could be found for $\hat{\theta}$ and therefore simulated annealing is employed to numerically optimize the log-likelihood function in (6.16). The optimization starts globally to avoid getting stuck in local minima at an early point, but this is still a possibility further on in the algorithm and therefore the initial guess of a starting point matter. To avoid achieving a local minimum from our optimization the algorithm was initiated with 10 different randomly chosen values for each estimation. If the results differed the $\hat{\theta}$ that yielded the maximum value of $\log\ p_x(x_1, x_2, ..., x_M|\theta; \hat{\lambda}, \hat{\tau}_1^{min}$ was chosen. A small clause was also made in our optimization algorithm if α was assigned a value close to 0 or 1 to remove those estimations since they aren't reasonable. If so was the case, the values for $\Delta\tau$ were also removed but the ones for τ_p^{max} were accounted for as reliable.

6.1.4 Properties of the AV model

The bimodality of the PDF is due to the two pathways and is clear when $\Delta\tau \gg 0$ and α is not close to its limit values. If $\Delta\tau$ approaches 0, the two peaks will merge and thus, visual inspection of the PDF is not necessarily a good way to judge if dual pathways are present or not. The amplitude and position of the peaks are related to the probability for that pathway (α) and the time difference ($\Delta\tau$). Decreasing α results in an increasing amplitude of the second peak and increasing $\Delta\tau$ shifts the second peak to the right. In Fig. 6.5 it is illustrated how the PDF becomes unimodal when α approaches 0 or 1, or when $\Delta\tau$ is close to 0.

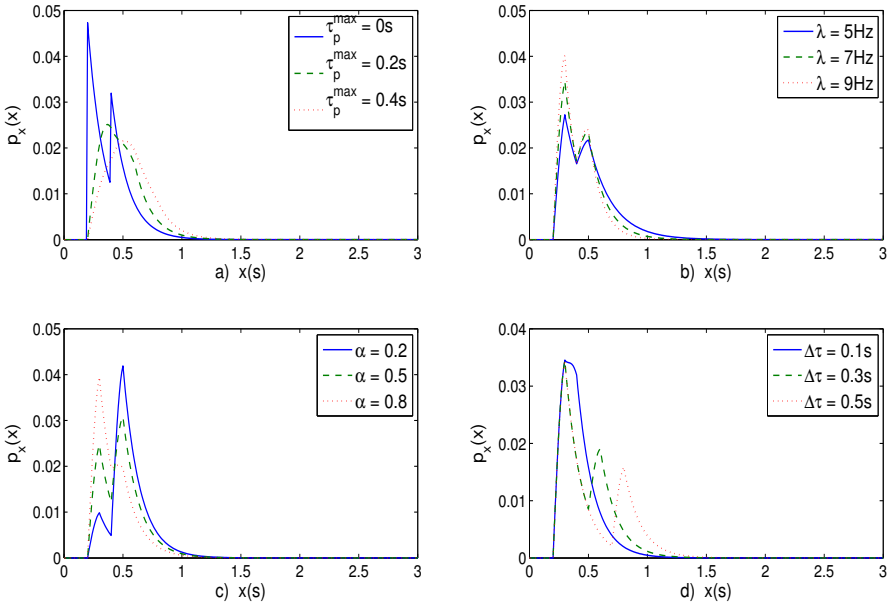

Figure 6.5: Properties for the PDF of the AV model for different values of a) τ_p^{max}, b) λ, c) α and d) $\Delta\tau$, where $x(s)$ is the length of the RR intervals. When the parameters were not subject to alteration the values were set to $\tau_p^{max} = 0.1$ s, $\lambda = 7$ Hz, $\alpha = 0.7$ and $\Delta\tau = 0.2$ s.

λ and τ_p^{max} affect the width of the peaks in such a way that increasing values of τ_p^{max} or decreasing values of λ broaden the peak. τ_p^{max} has a significant influence on the width, unlike λ who just have a limited effect as long as its within the physiological range.

6.2 Model modification

The model is modified before using it on the recorded ECG signals. The parameters that affect the modification are

λ - when estimating λ from the ECG-recordings some of the calculations result in $\lambda = NaN$. λ is calculated for every 10 s and we use the median for all in a 30-min segment, we set a restriction that more than 50 % of the calculated λ is not allowed to be NaN.

τ_1^{min} - if this parameter cannot be estimated from the Poincaré plot then no optimization can be done for that segment.

s_τ - the same as for τ_1^{min} but with the addition that it is not allowed to be larger or less than $\mu \pm \sigma$.

α - is not allowed to be larger than 0.99 or less than 0.01 since it is not physiologically probable.

The output from the new model are the estimated parameters only for the 30-min segments where all of these restrictions are fulfilled, which according to us are accounted for as reliable parameters to draw conclusions from.

Chapter 7

Performance evaluation

Evaluation of the model was done with both simulated and ECG-derived RR intervals. Simulated RR intervals were used to derive how many were necessary to get a good estimate of θ and to evaluate how changes in λ and τ_1^{min} affected the different output parameters. The latter analysis gives information on how a certain error propagates.

7.1 Simulated RR series

To evaluate the model used in this project both simulated and ECG-derived RR intervals were used. Simulated RR intervals were used to evaluate how many intervals needed for accurate parameter estimation. 100 RR intervals, each with the length of 30-min were simulated, with the parameters to be estimated set to:

$\alpha = 0.7$

$\tau_p^{max} = 0.1$ s

$\Delta\tau = 0.2$ s

The input values were set to

$\lambda = 7$ Hz

$s_\tau = 0.1$

$\tau_1^{min} = 0.2$ s

The aim with this part of the analysis was to evaluate the MLE created in this study and therefore s_τ and τ_1^{min} were not estimated, since that part

is created by Corino et al. [3]. The absolute error ϵ of the estimates were calculated for increasing lengths of the RR series, starting at 170 intervals increasing to 500 in steps of 10. The RR intervals were taken randomly from each 30-min recording and the mean of all absolute error values was calculated. When ϵ dropped below a predefined threshold, here set to 0.03 for both $\Delta\tau$ and τ_p^{max} and 0.05 for λ, the estimation was judged as accurate. These threshold values where chosen by [3] since they imply negligible changes in the PDF, and the same thresholds were used in this project.

Perturbation analysis was done to evaluate how changes in the input parameters affected the outcome. For this one 30-min segment of simulated RR intervals was used. The inputs were set to:

$$\boldsymbol{\lambda} = 7 \pm 1 \text{ Hz}$$
$$\boldsymbol{\tau}_1^{min} = 0.2 \pm 0.03 \text{ s}$$

The range of λ was set to reflect physiological changes, whereas the τ_1^{min}- range was the threshold for accuracy. 100 RR series, each containing 30 min recording, were used and the mean of all the estimated values were calculated.

Simulated RR series were also used to assess how to best carry through the performance evaluation for ECG derived RR intervals. The goal was to compare the models PDF with a wavelet-based density estimation calculated from the RR intervals. Different wavelet functions were compared to the PDF, to evaluate which gave the best fit.

7.2 ECG recordings

To evaluate how good the estimated PDF, $p_x(x|\hat{\boldsymbol{\theta}}; \hat{\lambda}, \hat{\tau}_1)$, was for modeling different RR series, the PDF was compared to a wavelet-based estimation of the real density function, $\tilde{p}_x(x)$. The reason for using a wavelet estimation is because nothing is known about the true PDF of the ECG-derived RR intervals, and the histogram has poor statistical properties [3]. The RR intervals that are used to compute $\tilde{p}_x(x)$ are the ones that have been transformed with s_τ to fit (6.8).

The key idea with the wavelet transform is to reduce the density problem to a fixed-design regression model [36]. The first step is to transform the sample X, in this case the RR intervals $x_1, x_2, ..., x_M$, into $y_1, y_2, ..., y_N$ using a binning procedure where $N = M/4$ and y_i is the number of samples in bin i. Then a wavelet decomposition into an optional number of levels is performed

using fast algorithm. The wavelet coefficients are then thresholded and used to reconstruct $\tilde{y}_1, \tilde{y}_2, ..., \tilde{y}_N$.

We chose the Symlet-6 wavelet with four levels for our evaluation. The six stands for the number of vanishing moments in the wavelet and the level is the number of coefficients it is decomposed into. The coefficients were then thresholded according to a soft data-dependent method. These settings produce a density that is a bit irregular but follows the histogram very thoroughly. Even though other settings gave smoother densities these settings were the ones that had the best accuracy with the correct PDF when we did the evaluation mentioned above. The accuracy of the estimated PDF's for the different RR series were evaluated in a measure of fit, U, in terms of percentage

$$U = 100 \cdot \left(1 - \int_0^3 |p_x(x|\hat{\boldsymbol{\theta}}; \hat{\lambda}, \hat{\tau}_1) - \tilde{p}_x(x)|dx\right) \tag{7.1}$$

The upper limit of the integral is set to three since since it is very rarely that RR intervals are longer than three s. To be able to compare $p_x(x|\hat{\boldsymbol{\theta}}; \hat{\lambda}, \hat{\tau}_1)$ with the wavelet-estimated PDF, $\tilde{p}_x(x)$ was created by interpolating the output of the wavelet estimation, $\tilde{y}_1, \tilde{y}_2, ..., \tilde{y}_N$.

The model was evaluated on the baseline recordings for all patients used in this analysis for each of the 30-min segments that were judged as accurate. Which these are can be found in the next section. All in all this resulted in 28 segments. An accuracy of $U > 80\%$ is considered to be an accurate model fit in [3].

Chapter 8

Drug analysis

The analysis consisted of comparing the baseline recordings from the patients with the recordings where they had taken Carvedilol, Diltiazem, Verapamil and Metoprolol, respectively. As mentioned above the data consisted of 24-hour recordings. The drugs did not affect the patients during the whole day and therefore the span where the drugs had their maximum effect, an interval of three hours, was chosen for further analysis. To investigate how the different parameters varied normally during a day a comparison was carried out for the baseline recordings between two different time intervals.

RR intervals preceding and following ectopic and wrongly detected beats were excluded from further analysis. The method for doing so was created by [3] using a method described in [37] and is based on heartbeat morphology. This analysis does not take circadian rhythm into consideration because the span is not so long that the circadian rhythm should affect the signals significantly and because the same hours of the day are compared against each other. The interval of interest was divided into six consecutive 30-min segments for all patients. Each of the 30-min segments were then analyzed with the slightly modified model where more restrictions had been added.

All patients that had recordings where at least 50 % of the segments in the interval of interest passed the new restriction, and where one of the recordings was the baseline measurement, were used in this study. This resulted in four patients for the analysis of Carvedilol and five patients for Diltiazem, Verapamil and Metoprolol respectively. The mean and standard deviation for the optimized parameters, $\theta = (\alpha, \Delta\tau, \tau_e^{max})$, during the interval was calculated for each patient for both the baseline and drug recordings. The cumulative mean and standard deviation were also computed for each measurement.

Chapter 9

Results

The results for the estimated AV nodal parameters are presented in the following chapter together with the results for the performance evaluation. First the evaluation of the model on simulated RR intervals will be treated, thereafter how well the estimated PDFs fit the RR interval histograms of the analyzed ECG segments and finally how the estimated parameters are affected by the different drugs.

9.1 Simulated RR series

In Fig. 9.1 the histogram of a segment of simulated RR intervals is displayed with its true and estimated PDF. When only $\hat{\theta}$ was estimated it resulted in values that only differed in the third decimal from the correct solution, and a PDF that is almost identical to the true one. In the case when $\hat{s}_\tau$ and $\hat{\tau}_1^{min}$ also were estimated the resulting PDF differ slightly from the true one. The parameter differences were though still below the threshold values.

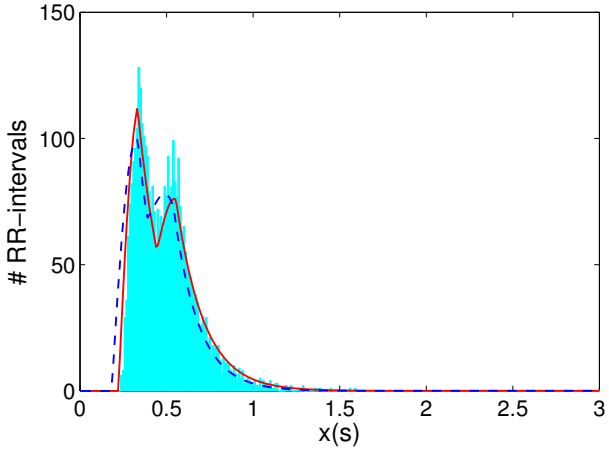

Figure 9.1: The true (solid line) and estimated PDF (dashed line) superimposed on the histogram of the transformed simulated RR intervals, where $\lambda = 7$ Hz, $s_\tau = 0.1$ s, $\tau_1^{min} = 0.2$ s, $\alpha = 0.7$, $\Delta\tau = 0.2$ s and $\tau_p^{max} = 0.1$ s. In a) only $\hat{\theta}$ is estimated, and in b) $\hat{s}_\tau$, $\hat{\tau}_1^{min}$ and $\hat{\theta}$ is estimated.

To evaluate how many RR intervals that were required for getting accurate estimates, 100 RR segments were simulated with defined parameter settings (see Fig. 9.2). An average absolute error was calculated for the parameter estimates for all these RR segments. Since 170 RR intervals at least are needed for estimating $\hat{s}_\tau$ from the Poincaré plot, 170 was set to the least number of intervals investigated. In this evaluation the optimization was limited to $\hat{\theta}$ for assessing how accurate that part of the MLE was. The MLE is judged to work accurately for 200 RR intervals or more. In the drug analysis of this study 30-min segments are used which contains many more than 200 intervals.

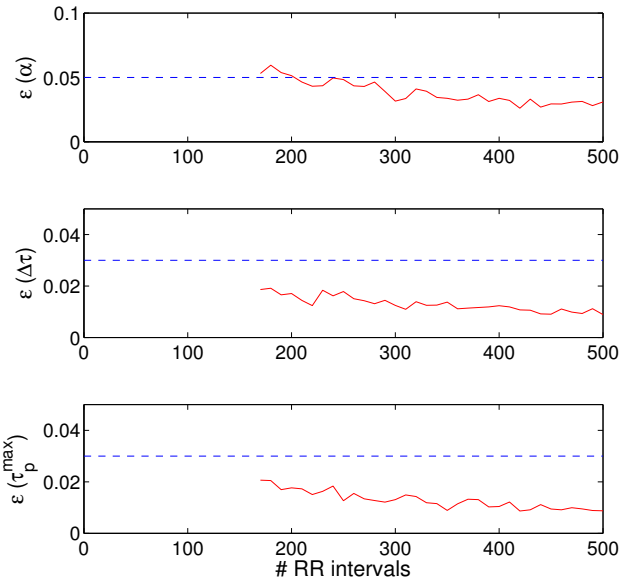

Figure 9.2: The average absolute error, ϵ, obtained from 100 different simulated RR segments with $\lambda = 7$ Hz, $\alpha = 0.7$, $\Delta\tau = 0.2$ s and $\tau_p^{max} = 0.1$ s. The dashed lines represent the thresholds below which the estimations are judged as accurate.

Since λ and τ_1^{min} are estimated in advance it is of interest to investigate the effect on the estimation of θ due to small errors in these parameters. A median for θ from 100 simulated RR series, the settings for these can be found in Fig. 9.3, with the length of 500 intervals was calculated for each change. λ was changed $\pm$ 1 Hz and τ_1^{min} $\pm$ 0.03 s. None of the changes resulted in large errors. As can be seen in Fig. 9.3 all of the estimates are within the thresholds when changing λ. Changes in τ_1^{min} affect a bit more, an increase of 0.03 s results in a decrease of 0.06 s τ_p^{max}, but the changes in $\hat{\alpha}$ and $\Delta\hat{\tau}$ are more probable to be due to normal estimation differences than to the change in τ_1^{min}.

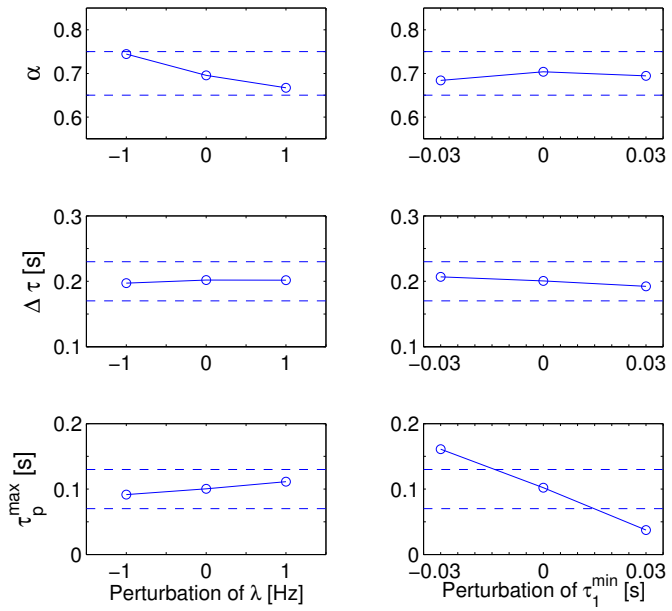

Figure 9.3: Effects of perturbation of λ and τ_1^{min} on the estimates of α, $\Delta\tau$ and τ_p^{max}. The median (solid line) of the estimates were calculated from 100 simulated RR series, created using $\lambda = 7$ Hz, $\tau_1^{min} = 0.1$ s, $\alpha = 0.7$, $\Delta\tau = 0.2$ s and $\tau_p^{max} = 0.1$ s. The dashed lines show within which interval the parameters of $\hat{\theta}$ are judged as accurate.

9.2 ECG recordings

The distribution of how good the estimated PDFs are, U, is shown in Fig. 9.4. The evaluation is so far done on all 30-min segments for the baseline recordings, but will be increased to include all 30-min segments for the study. The predefined threshold for an accurate fit is only fulfilled for 46 % of the segments.

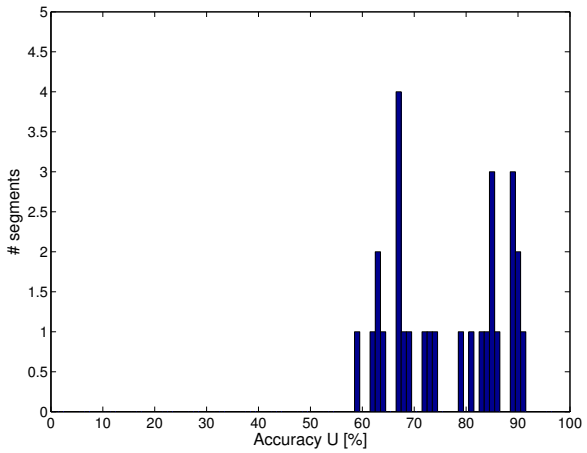

Figure 9.4: Distribution of the measure of fit, U in %, evaluated for 28 different 30-min ECG segments. The mean is 77 % with standard deviation 11 %.

Figures 9.5 and 9.6 show different cases of an estimated PDF superimposed on a transformed RR segment. In Fig. 9.5 two visually very good estimates are shown in (a) and (c). In (b) an example of how the PDF is slightly shifted is shown, a problem that occurred from time to time. The plot in (d), shows another problem that we had with our estimates, sometimes the smaller peak was missed. For a few segments the RR segments resulted in histograms with three peaks, see Fig. 9.6 (a). Our model is developed to take one or two peaks into account and therefore these estimates were partly inaccurate. In (b) it is shown that the PDFs adjusted well when only one peak was present.

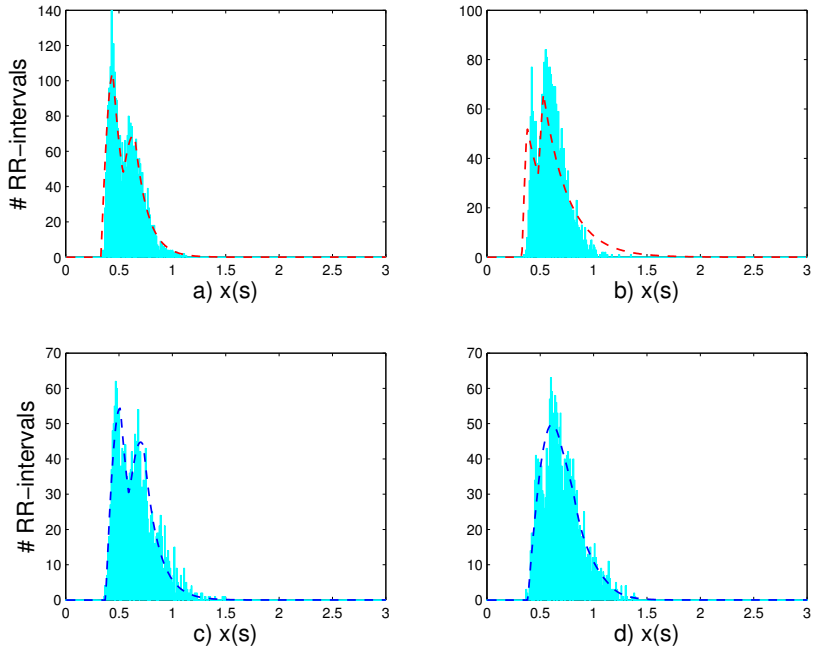

Figure 9.5: Four different transformed RR segments with the estimated PDF superimposed (dashed line) from one patient. a) An accurate estimation for a baseline recording. b) An estimate for the next half hour of the same recording where the PDF is slightly shifted to the right from the histogram c) An accurate estimate for a Metoprolol recording. d) An estimate where the second peak is missed, done for the same recording one hour later.

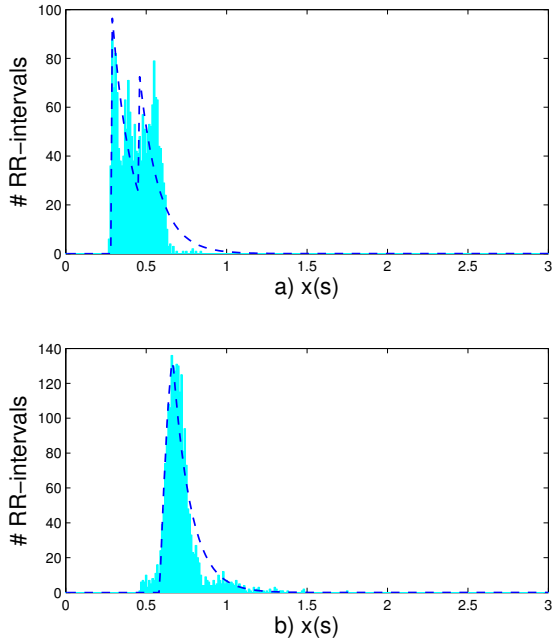

Figure 9.6: Histogram of transformed RR segments from the same patient. a) A baseline recording, problem occurred when the histogram had three peaks. b) A Metoprolol recording, the PDF adjusted well for a single high peak.

9.3 Drug analysis

Figures 9.7, 9.8, 9.9 and 9.10 display the means and standard deviations of $\hat{\theta}$ for each patient, for both baseline and drug recordings, and the cumulative values. The analysis is done with the recordings that fulfilled the modified MLE. This generated in four patients for the Carvedilol study and five patients for each of the other drugs.

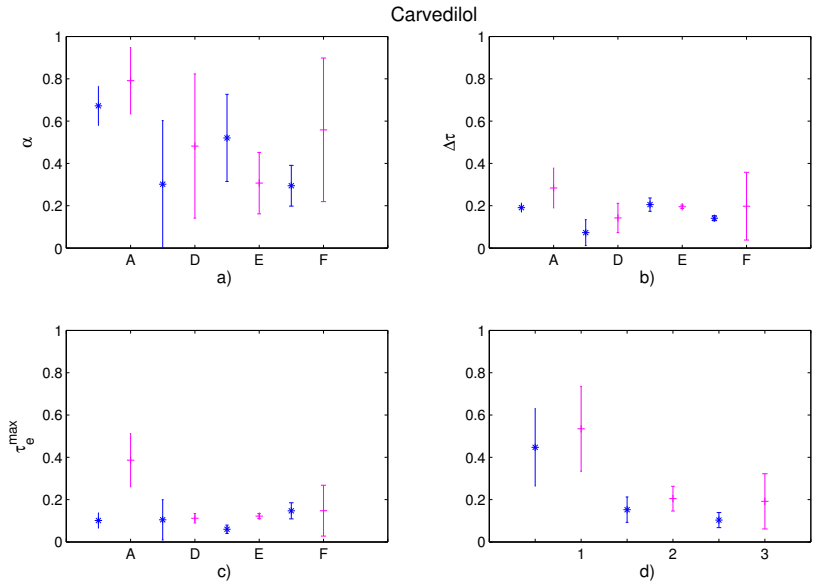

Figure 9.7: Comparison between baseline (*) and Carvedilol (-) parameters. In a)-c) the mean and standard deviation for all parameters of $\hat{\theta}$ are displayed for each patient, (A, D, E and F). d) The cumulative means and standard deviations for $1 = \hat{\alpha}$, $2 = \Delta\hat{\tau}$ and $3 = \tau_p^{max}$ for all patients in this study.

In Fig. 9.7 the results for Carvedilol are displayed. In general all parameters increased when Carvedilol was active, compared to baseline, $\hat{\alpha}$ with 0.08, $\Delta\hat{\tau}$ with 0.05 s and $\hat{\tau}_p^{max}$ with 0.09 s. But important to note is that for τ_p^{max} the standard deviation increased too.

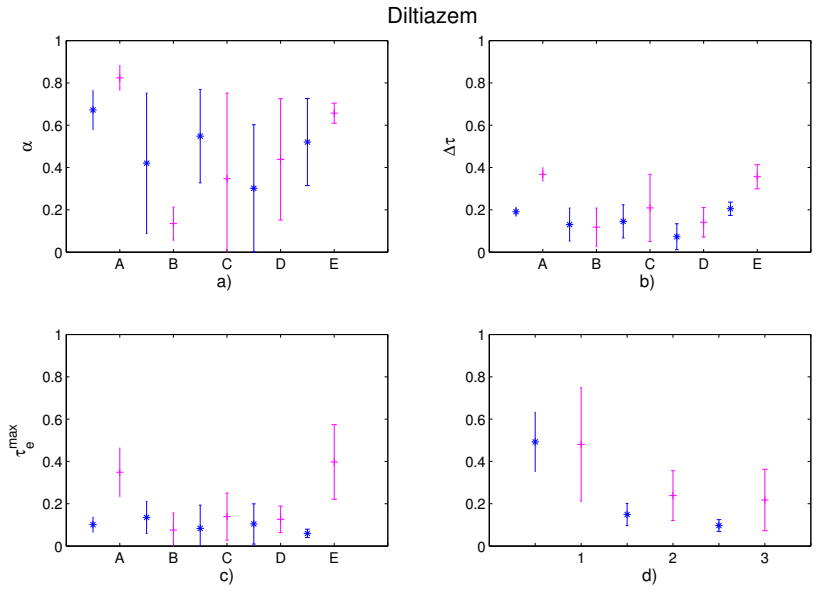

Figure 9.8: Comparison between baseline (*) and Diltiazem (-) parameters. In a)-c) the mean and standard deviation for all parameters of $\hat{\theta}$ are displayed for each patient, (A - E). d) The cumulative means and standard deviations for $1 = \hat{\alpha}$, $2 = \Delta\hat{\tau}$ and $3 = \tau_p^{max}$ for all patients in this study.

Diltiazem did not affect the average probability of choosing either pathway,which can be seen in Fig. 9.8, for some patients the drug increased the probability of the fast pathway and for some it decreased. Both the means and standard deviations for $\Delta\hat{\tau}$ and $\hat{\tau}_p^{max}$ increased, 0.09 ± 0.07 s and 0.12 ± 0.12 s respectively.

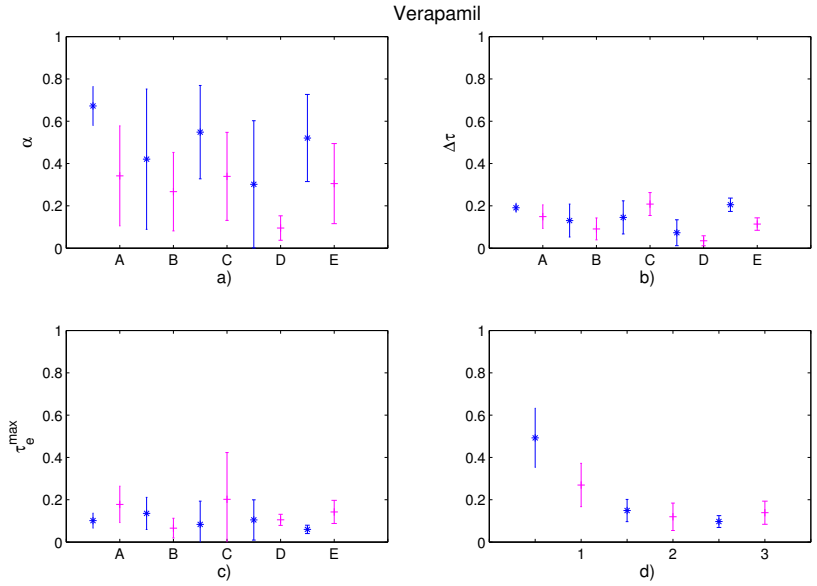

Figure 9.9: Comparison between baseline (*) and Verapamil (-) parameters. In a)-c) the mean and standard deviation for all parameters of $\hat{\theta}$ are displayed for each patient, (A - E). d) The cumulative means and standard deviations for $1 = \hat{\alpha}$, $2 = \Delta\hat{\tau}$ and $3 = \tau_p^{max}$ for all patients in this study.

The effect on $\hat{\theta}$ caused by Verapamil can be found in Fig. 9.9. Verapamil lowered the probability of the signal taking the longer pathway, $\hat{\alpha}$, with 0.22. It also lowered the mean of $\Delta\hat{\tau}$ with 0.03 s, a trend that is visual also when looking at the results for each patient. The drug slightly increased $\hat{\tau}_p^{max}$ with 0.04 s.

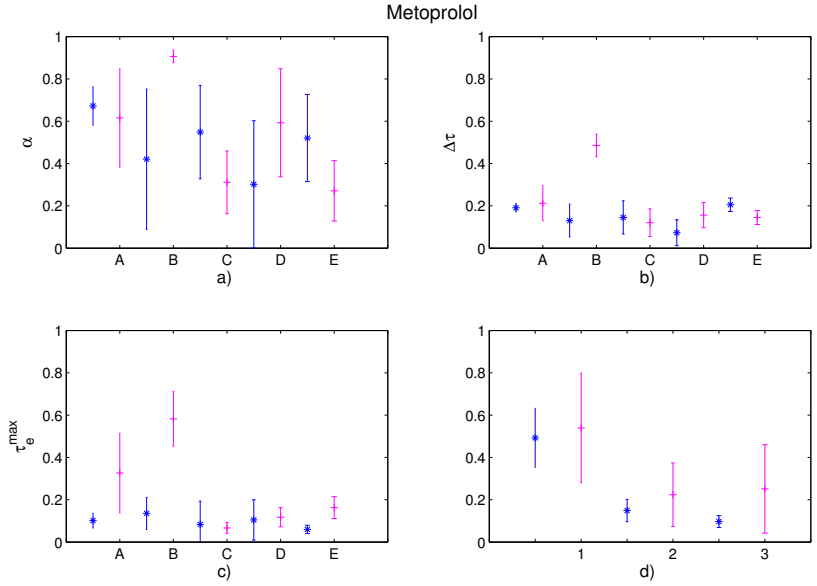

Figure 9.10: Comparison between baseline (*) and Metoprolol (-) parameters. In a)-c) the mean and standard deviation for all parameters of $\hat{\theta}$ are displayed for each patient, (A - E). d) The cumulative means and standard deviations for $1 = \hat{\alpha}$, $2 = \Delta\hat{\tau}$ and $3 = \tau_p^{max}$ for all patients in this study.

It can be seen in Fig. 9.10 that the effect of Metoprolol varied from patient to patient. It had a marked effect on patient B where all parameters increased, $\hat{\alpha}$ with as much as 0.49 making it very probable for the signals to take the longer pathway. For patient C on the other hand the effect was a little bit more modest but here all parameters decreased. The cumulative mean for all parameters of $\hat{\theta}$ increased, but so did also the standard deviation and the new span included both higher and lower values than baseline.

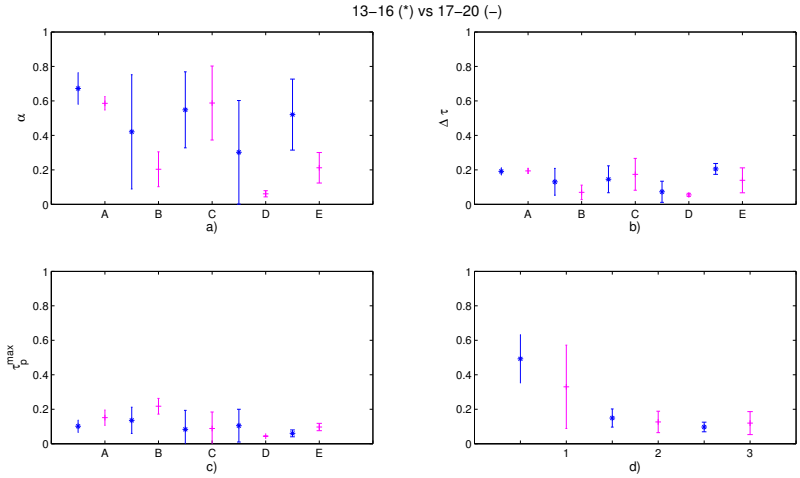

Figure 9.11: Comparison between baseline at 1 pm to 4 pm (*) and baseline at 5 pm to 8 pm (-) parameters. In a)-c) the mean and standard deviation for all parameters of $\hat{\theta}$ are displayed for each patient, (A - E). d) The cumulative means and standard deviations for $1 = \hat{\alpha}$, $2 = \Delta\hat{\tau}$ and $3 = \tau_p^{max}$ for all patients in this study.

In Fig. 9.11 the comparison between two different time intervals for the baseline recordings is shown. It is visual that both τ_{max}^p and $\Delta\tau$ were quite stable for all patients, whereas α varied. The change of α was independent but for most patient the trend was a decrease from the first time interval to the second, later one.

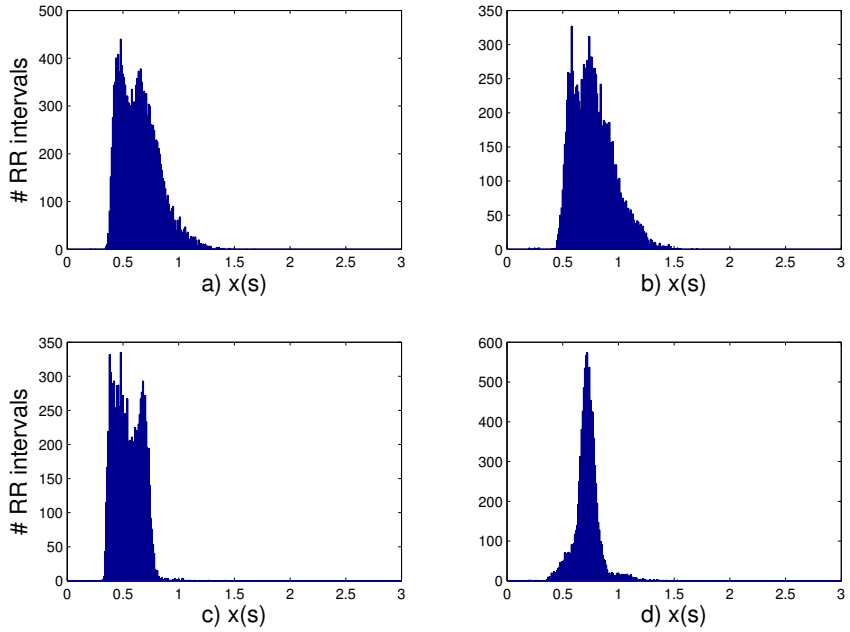

Figure 9.12: Histogram of RR intervals. a) Displays histogram for patient A during baseline recordings and b) during Metoprolol. c) Displays histogram for patient C during baseline recordings and d) during Metoprolol.

To see whether the histograms of the analyzed segments changed according to how the change in estimated parameters would predict them to Fig. 9.12 shows the plot for two of the patients during baseline and Metoprolol recordings. For patient C the histogram is shifted to the right, towards longer RR intervals, and gets much more narrow. The histogram for patient A has a more subtle shift towards the longer RR intervals.

Chapter 10

Discussion

One of the largest problems encountered in this study was the large number of λ's not computed correctly, resulting in a large amount of NaN (Not a Number). Since these calculations were not a part of this study, the problem was solved by putting a threshold of acceptable number of NaNs. This threshold was set to 50%, at least half of the λ's in every half hour had to have a value for the half hour to be included in the evaluation. A higher threshold excluded too many patients, and 50 % was the lowest threshold decided to be statistical inacceptable. The original ECG signals were briefly examined for noise. Small fibrillary waves can sometimes disappear in noise, but large noise could not be found in the recordings evaluated in this study. It should be noted that these examinations where performed visually for short segments of the ECG recordings and are not scientifically secured.

For future analysis the background to this problem should be evaluated more thoroughly. The signals should be evaluated for noise and the QRST cancellation should also be looked over for errors or improvements. Noise could be due to the ambulatory conditions or bad setup of the recording equipment. One suggestion could be to use the new method by Petrenas et al. [20] in Sec. 3.1.6. since it has shown better results than an average beat subtraction method.

The two other parameter that were estimated independently of the output were s_τ and τ_1^{min}. Of these, s_τ was not assigned any restriction. For further studies perturbation analysis could be carried out to see how small errors affects the result, and an analysis of how much s_τ does change during the day to evaluate whether it should be restricted or not. The restriction on τ_1^{min} should accept 95 % of the values, if they are normally distributed, and

only delete outliers caused by estimation errors since the parameter does not have a wide span of probable values and is therefore justified.

In the algorithm there is a restriction so that α is not assigned unphysiological values. Since the ML estimation of θ sometimes generate these values it can be an indication that the optimization from time to time gets stuck in local minima. One way in trying to diminish this problem could be to run simulated annealing more times before choosing the best values or adjust it more for the task, in this study Matlab's default features are used. Another way could be to look into other optimization methods.

The drugs analyzed in this study are all supposed to act by increasing the AV nodal block that should result in longer RR intervals. Thus, a decrease in α is expected. As seen in Fig. 6.5, a decrease in α gives a higher probability for the signal to take the fast pathway and increasing the height of the second peak.

When evaluating the RR interval histograms for changes due to the drugs (see Fig. 9.12), a small shift to the right is seen for both patient A and C for recordings with Metoprolol. The two peaks clearly merges into one for patient C, whereas a merge of the peaks are not distinct for patient A. Since longer RR intervals are desired as a result of medication, these results are not all in agreement. Looking at the results of perturbation analysis shown in Fig. 6.5, a shift to the right should indicate a decrease in α resulting in longer RR intervals. A merge of the two peaks should indicate a decrease in $\Delta\tau$, which is not desirable since an increase in $\Delta\tau$ should give the possibility for longer RR intervals. As seen in Fig. 9.10 α is decreasing for both patient A and C and $\Delta\tau$ is affected significantly.

In Fig. 9.7 it is seen that for Carvedilol, α and $\Delta\tau$ increased for three out of four patients and τ_p^{max} increased for all of the patients. The results for α are not in agreement with what is expected. As mentioned above an increase in α gives a higher probability for impulses taking the slower pathway, that results in larger amount of short RR intervals. Since the same change in α is seen for a majority of the patients, it is excluded that these results are due to ambulatory conditions or interference in the recording. The results for $\Delta\tau$ and τ_p^{max} though, indicates what is expected, an increased $\Delta\tau$ increases the time between the shorter and longer RR intervals and since τ_1^{min} is fixed the longer intervals are those who are affected. An increased τ_p^{max} results in a higher probability for longer RR intervals, also in agreement with the expectations.

Almost the same results are shown for Diltiazem in Fig. 9.8 where α

increased for three patients and decreased for two, which gave a mean of minimal change. Note that all patients do not get the same result for these two drugs, for example patient E where α decreases with Carvedilol but increases with Diltiazem. Verapamil had the same effect for most patients, as well as Carvedilol, whereas the effect of Metoprolol and Diltiazem varies more from patient to patient. Our investigation of normal changes in the parameters during the day showed that α varied a lot while the other two parameters were more consistent. This indicates that the changes in α might also be affected by daily variation, while the effect on τ^p_{max} and $\Delta\tau$ is mostly due to the drugs.

The drugs are obviously affecting the patients in different ways and with different effect and since the recordings were ambulatory, changes due to patients activity may occur. It is taken as an indication of how each drug affects the parameters of interest, when the same drug effects are seen in several patients and they are more marked than normal daily variation.

The results are accounted for as statistically reliable due to the process of assessing them. The study started out with 12 patients from which the AF frequency was estimated. The screening process was then applied to all of the patients and only the ones that fulfilled the requirements where taken further in the analysis. Because of the challenges in analyzing AF it may be difficult to have a large patient group, and earlier studies have also been restricted to base their studies on a few number of participants [1]. But to get a greater certainty, more patients should be evaluated or the patients activity during the recordings should be documented to give as good comparison as possible.

Our results show a strong variance in the effect of each drug for different patients, a problem that would be desirable to solve to facilitate treatment of AF. One interesting approach would be to evaluate more of the patients characteristics, such as heart rate, AF durability, age etc. to see if the different drug effects are associated with the patients characteristics and how to measure these.

Chapter 11

Conclusion

In this study a statistical method for quantitatively analyzing the effects of AF drugs is presented. The model focuses on the electrical activity in the AVN and accounts for several physiological characteristics such as dual nodal pathways, concealed conduction and relative refractoriness. The parameters that are estimated and analyzed are the probability of the atrial signal to take the longer pathway, the difference in refractory period between the two pathways and the maximum prolongation.

A measure of fit evaluation showed that the model has a mean accuracy of 77 %, with a standard deviation of 11 %. These values are a bit low, which should be noted when interpreting the results. But due to the robustness in the model for the performance evaluation the results are still accounted for as reliable.

The statistical analysis of recorded ECG signals, for patients both under the influence of AF drugs and without, show visual effects in all estimated parameters. The results differ between drugs, and sometimes between patients, but for most of the drugs a trend of the changes can be made out. The drugs mostly caused more marked effects in the parameters than normal daily variation.

This study indicates that the model is applicable for assessing quantitative results of how antiarrhythmic drugs influence AF patients. There are certain aspects of the model that need improvement, e.g. a more robust method for estimating the fibrillation frequency and other optimization methods.

Bibliography

[1] L. Mangin, A. Vinet, P. Pagé, and L. Glass, "Effects of antiarrhythmic drug therapy on atrioventricular nodal function during atrial fibrillation in humans," *Europace*, vol. 7 Suppl. 2, pp. 71–82, 2005.

[2] R. J. Cohen, R. D. Berger, and T. E. Dushane, "A quantitative model for the ventricular response during atrial fibrillation," *IEEE Trans. Biomed. Eng.*, vol. 30, no. 12, pp. 769–781, 1983.

[3] V. Corino, F. Sandberg, L. Mainardi, and L. Sörnmo, "An atrioventricular node model for analysis of the ventricular response during atrial fibrillation," *IEEE Trans. Biomed. Eng.*, vol. 58, pp. 3386 – 3395, 2011.

[4] L. Sörnmo and P. Laguna, *Bioelectrical signal processing in cardiac and neurological applications.* Elsevier Academic press, 2005.

[5] D. Brooks and R. MacLeod, "Electrical imaging of the heart," *Signal Processing Magazine, IEEE*, vol. 14, no. 1, pp. 24 –42, 1997.

[6] L. Mainardi, L. Sörnmo, and S. Cerutti, *Understanding Atrial Fibrillation: The Signal Processing Contribution.* Morgan and Claypool, 2008, ch. 1.

[7] A. Bollmann and F. Lombardi, "Electrocardiology of atrial fibrillation," *Engineering in Medicine and Biology Magazine, IEEE*, vol. 25, no. 6, pp. 15 –23, 2006.

[8] L. Mainardi, L. Sörnmo, and S. Cerutti, *Understanding Atrial Fibrillation: The Signal Processing Contribution.* Morgan and Claypool, 2008, ch. 5.

[9] F. L. Meijler, J. Jalife, J. Beaumont, and D. Vaidya, "Av nodal function during atrial fibrillation: the role of electrotonic modulation of

propagation," *J. Cardiovasc. Electrophysiol.*, vol. 7, no. 9, pp. 843–861, 1996.

[10] R. Langendorf, "Concealed a-v conduction; the effect of blocked impulses on the formation and conduction of subsequent impulses," *Am Heart J*, vol. 35, no. 4, pp. 542–552, Apr 1948.

[11] C. Antzelevitch and G. K. Moe, "Electrotonic inhibition and summation of impulse conduction in mammalian purkinje fibers," *Am J Physiol*, vol. 245, no. 1, pp. 42–53, Jul 1983.

[12] J. M. Davidenko, M. Delmar, J. Beaumont, D. C. Michaels, P. Lorente, and J. Jalife, "Electrotonic inhibition and active facilitation of excitability in ventricular muscle," *J Cardiovasc Electrophysiol*, vol. 5, no. 11, pp. 945–960, Nov 1994.

[13] Y. Liu, W. Zeng, M. Delmar, and et al, "Ionic mechanisms of electrotonic and concealed conduction in rabbit atrioventricular nodal myocytes," *Circulation*, vol. 88, pp. 1634–1646, 1993.

[14] G. K. Moe, J. B. Preston, and H. Burlington, "Physiologic evidence for a dual a-v transmission system," *Circ Res*, vol. 4, no. 4, pp. 357–375, Jul 1956.

[15] Y. Zhang, S. Bharati, K. A. Mowrey, S. Zhuang, P. J. Tchou, and T. N. Mazgalev, "His electrogram alternans reveal dual-wavefront inputs into and longitudinal dissociation within the bundle of his," *Circulation*, vol. 104, no. 7, pp. 832–838, Aug 2001.

[16] A. M. Climent, M. S. Guillem, Y. Zhang, J. Millet, and T. N. Mazgalev, "Functional mathematical model of dual pathway av nodal conduction," *Am J Physiol Heart Circ Physiol*, vol. 300, no. 4, pp. 1393–1401, Apr 2011.

[17] M. P. Ingemansson, J. Carlson, and S. B. Olsson, "Modification of intrinsic av-nodal properties by magnesium in combination with glucose, insulin, and potassium (gik) during chronic atrial fibrillation," *J. Electrocardiol*, vol. 31, no. 4, pp. 281–292, 1998.

[18] J. Slocum, E. Byrom, L. McCarthy, A. Sahakian, and S. Swiryn, "Computer detection of atrioventricular dissociation from surface electrocardiograms during wide qrs complex tachycardias," *Circulation*, vol. 72, no. 5, pp. 1028–1036, 1985.

[19] L. Mainardi, L. Sörnmo, and S. Cerutti, *Understanding Atrial Fibrillation: The Signal Processing Contribution.* Morgan and Claypool, 2008, ch. 3.

[20] A. Petrenas, V. Marozas, L. Sörnmo, and A. Lukosevicius, "Atrial activity extraction during atrial fibrillation using reservoir computing," 2012, presented during Medicinteknikdagarna in Lund, 2012.

[21] [Online]. Available: http://www.mathworks.se/help/signal/ref/spectrum.welch.html

[22] F. Sandberg, M. Stridh, and L. Sörnmo, "Frequency tracking of atrial fibrillation using hidden markov models," *IEEE Trans. Biomed. Eng.*, vol. 55, no. 2 Pt 1, pp. 502–511, 2008.

[23] J. Lian, D. Müssig, and V. Lang, "Computer modeling of ventricular rhythm during atrial fibrillation and ventricular pacing," *IEEE Trans. Biomed. Eng.*, vol. 53, no. 8, pp. 1512–1520, 2006.

[24] P. Jorgensen, C. Schäfer, P. G. Guerra, M. Talajic, S. Nattel, and L. Glass, "A mathematical model of human atrioventricular nodal function incorporating concealed conduction," *Bull. Math. Biol.*, vol. 64, no. 6, pp. 1083–1099, 2002.

[25] C. Luo and Y. Rudy, "A model of the ventricular cardiac action potential," *Circ. Res.*, vol. 68, pp. 1501–1526, 1991.

[26] G. Lindgren, H. Rootzén, and M. Sandsten, "Stationary stochastic processes," 2010.

[27] H. Larson and B. Shubert, *Probabilistic Models in Engineering Sciences: Random Variables and Stochastic Processes, vol. 2.* New York: John Wiley and Sons Inc., 1979.

[28] G. Blom, J. Enger, G. Englund, J. Grandell, and L. Holst, *Sannolikhetsteori och statistikteori med tillämpningar.* Studentlitteratur, 2005.

[29] S. Kay, *Fundamentals of Statistical Signal Processing. Estimation Theory.* New Jersey: Prentice-Hall, 1993.

[30] [Online]. Available: http://www.mathworks.se/discovery/simulated-annealing.html

[31] S. Kirkpatrick, C. D. Gelatt, and M. P. Vecchi, "Optimization by simulated annealing," *Science*, vol. 220, no. 4598, pp. 671–680, 1983.

[32] [Online]. Available: http://www.mathworks.se/help/gads/how-simulated-annealing-works.html

[33] [Online]. Available: http://clinicaltrials.gov/show/NCT00313157

[34] [Online]. Available: http://www.1177.se/Ostergotland/

[35] V. Corino, F. Sandberg, F. Lombardi, L. Mainardi, and L. Sörnmo, "Atrioventricular nodal function during atrial fibrillation: Model building and robust estimation," 2012, accepted for publication in Biomed. Signal Proc. Control, 2013.

[36] M. version 7.11.0 (R2010b), *Wavelet Applications:Function Estimation: Density andd Regression.* Natick, Massachusetts: The Mathworks Inc., 2010.

[37] M. Lagerholm, C. Peterson, G. Braccini, L. Edenbrandt, and L. Sörnmo, "Clustering ecg complexes using hermite functions and self-organizing maps," *IEEE Trans. Biomed. Eng.*, vol. 47, no. 7, pp. 838–848, 2000.